Alexandria Engineering Journal (2021) 60, 2583–2605

Alexandria University

Alexandria Engineering Journal

www.elsevier.com/locate/aej
www.sciencedirect.com

Simulation of natural convective heat transfer and entropy generation of nanoparticles around two spheres in horizontal arrangement

Basma Souayeh [a,b,*], Fayçal Hammami [b], Najib Hdhiri [b], Mir Waqas Alam [a], Essam Yasin [a], Alaaedeen Abuzir [a]

[a] *King Faisal University, College of Science, Department of Physics, PO Box 400, Al-Ahsa 31982, Saudi Arabia*
[b] *University of Tunis El Manar, Faculty of Sciences of Tunis, Laboratory of Fluid Mechanics, Physics Department, 2092 Tunis, Tunisia*

Received 16 November 2020; revised 1 January 2021; accepted 4 January 2021
Available online 15 January 2021

KEYWORDS

Natural convection;
Heat transfer;
Nanoparticles;
Entropy generation;
Two horizontally arranged spheres

Abstract Herein, laminar convective heat transfer from two horizontally arranged spheres has been evaluated by using numerical models inside water-based fluids incorporated with alumina (Al_2O_3), copper oxide (CuO), and copper (Cu) nanoparticles. The problem was simulated for different Rayleigh numbers ranging from 10^3 to 10^6 and various volume fractions including 2, 4, 6, and 8%. The evaluation process included the perspective of both first and second thermodynamic laws. In-house FORTRAN code was provided to solve the equations based upon the finite volume method as well as the Multigrid acceleration. According to the obtained results, the average Nusselt number enhanced by 57.4% for both the spheres and plates with increment of the Rayleigh number from 10^3 to 10^6 for the constant volume fraction of 2%. In addition, nanoparticle type played a significant role on the heat transfer rate and generated entropy. Moreover, introduction of the Al_2O_3 nanoparticles into the water-based fluid resulted in approaching to the highest Bejan number of 0.98. Furthermore, the ecological coefficient of performance of CuO nanoparticles decreased by increment of the volume fraction at all Rayleigh numbers. In the volume fraction of 2%, it raised from 2.89 to 7.8 by increasing of the Rayleigh number from 10^3 to 10^6.

1. Introduction

Generally, a flow motion driven by gravity force is known as natural convection. Basically, the natural convection is resulted from the variance in the temperature as well as concentration of the fluid. Heat transfer process through natural convection has received tremendous attentions from numerous

* Corresponding author.
E-mail address: bsouayeh@kfu.edu.sa (B. Souayeh).
Peer review under responsibility of Faculty of Engineering, Alexandria University.

https://doi.org/10.1016/j.aej.2021.01.002

Nomenclature

Be	Bejan number
C_p	specific heat capacity ($Jkg^{-1}K^{-1}$)
D	width of the channel wall (m)
g	gravitational acceleration (ms^{-2})
H	distance between upper and lower wall of the channel (m)
k	thermal conductivity ($Wm^{-1}K^{-1}$)
L	length of the channel (m)
Nu	Average Nusselt number
n	normal direction
Pr	Prandtl number
P_0	Pressure scale, ρu_0^2
$\overrightarrow{q}$	Heat flux vector (w/m^2)
Ra	Rayleigh number
S^*_{gen}	adimensional generated entropy per unit volume (w/m^3k)
T_c	cold wall temperature (k)
T_h	hot wall temperature (k)
T	Temperature (k)
t	dimensionless time
u, v, w	dimensionless velocity components
x, y, z	dimensionless Cartesian coordinates

Greek symbols

ϕ	solid volume fraction
α	thermal diffusivity (m^2/s)
θ	dimensionless temperature, $\theta = (T-T_c)/(T_h-T_c)$
ν	kinematics viscosity (m^2/s)
μ	dynamic viscosity (kg /(m.s))
ρ	fluid density (kg/m^3)
β	coefficient of thermal expansion (K^{-1})
φ	Irreversibility coefficient
Ω	Global domain

subscripts

$*$	Dimensional variable
max	maximum
c	cold
h	hot
Avg	average
TG	thermal gradient
VG	velocity gradient
Loc	local
Tot	total

researchers and engineers. As an example, efficiency enhancement of the cooling systems has become a crucial issue due to reducing energy demand caused by growth of the small-sized devices. However, lack of coolant fluids with appropriate thermal conductivity has restricted approaching to the high-efficient cooling systems. So, several researchers have focused on applying of nanofluids to improve the cooling procedure. Commonly, nanofluids are consisted of nanoparticles dispersed in original water-based fluids. They are utilized as coolant fluids in a wide variety of applications including automotive devices, refrigerators, and power generators. Introduction of the nanofluids into the original base fluids results in the thermal conductivity enhancement as well as coefficient improvement of the convective heat transfer [1]. The reason may be assigned to higher thermal conductivity of the metallic or non-metallic particulate materials compared with that of the original base fluids which leads to enhancement of the heat transfer coefficient. Copper (Cu), alumina (Al_2O_3), and copper oxide (CuO) are of the known nanofluids applied in this regard [1,2]. Nanofluids are distinguished by several features including shape, volume fraction, particle size, stability, and thermophysical properties. The aforementioned characteristics play a prominent role in the heat transfer performance [3–9].

Heat transfer enhancement, entropy generation rising, and flow intensification have been represented through insertion of the nano particulate materials into the original base fluids in a number of literatures. In addition, the natural convection heat transfer phenomena from a single spherical body are one of the most fundamental structures commonly encountered in the heat-related researches [10–13]. Although, evaluation of the heat transfer phenomena in double-sphere structures is considered as a more representative technique. The reason could be corresponded to the interaction of contiguous structures included in a system. Yet, very few studies have examined the heat transfer phenomena under different boundary conditions.

Sheikholeslami et al. [14] summarized the important findings in the field of nanofluid domains. Based upon this research, several aspects of the nanofluids have been investigated including free convection phenomena in a porous cubical structure utilizing the lattice Boltzmann method, magnetic field effect on the nanofluids, and so on. The results have shown that the kinetic energy of the nanofluids enhanced resulting from increment of the Rayleigh number. Whilst, the Darcy number was reduced by increasing of the Hartmann number. A sphere incorporated with micro polar Cu and Al_2O_3 nanoparticles was applied by Swalmeh et al. [15] to examine flow of the natural convection in its boundary layer. They stated that Al_2O_3 water-based micro polar nanofluid revealed superior heat transfer rates as well as higher local skin friction compared with the one filled with Cu nanoparticles.

Alwawi et al. [16] used nanofluid of Sodium Alginate (SA-NaAlg) as a convection flow to investigate the magneto hydrodynamic flow over a solid sphere. Several types of nanofluids were applied to evaluate the impact of the nanoparticle features along with the magnetic field on the heat transfer procedure. The results showed that increment of the nanoparticles' volume fraction led to enhancement of the local Nusselt number and skin friction. In addition, the profiles of the temperature and velocity were improved by enhancement of the nanoparticles' volume fraction.

A. Baïri [17] applied a nanofluid immersed in a permeable media to enhance the warm plan of a circular electronic gadget. The gadget was located in the centre of another circular

device to make it isothermal. It has been demonstrated that the convective warmth motion was efficiently increased with the ratio of capacity to the Rayleigh number. In addition, the normal Nusselt number increased with the Rayleigh number. It is while, impact of the portion volume was in the percent range from 2 to 10%. Gupta et al. [18] utilized several nanoparticles consisting Al_2O_3, CuO, silica (SiO_2), and zinc oxide (ZnO) to explore the heat transfer from a warmed circle. In the mentioned examination, the temperature-subordinate conditions were applied for the consistency and warm conductivity of the nanofluids to represent the temperature effect on the various features. According to the obtained results, 20–30% improvement was observed for the warmth motion over the utilized normal Newtonian liquids which supposedly increased with the expanding estimations of the Peclet number. Recently, the laminar natural convection over an isothermal sphere has been performed by Yang et al. [19]. This investigation has been carried out through the SIMPLEC method in both steady and transient cases for different types of fluids. Base on the obtained data, the conductive heat transfer was predominant when the sphere was located within a cold fluid. Nepal et al. [20] evaluated the influence of a convection flow over a sphere heated internally. A laminar and unsteady flow was used in this examination. As a higher internal heat was utilized, a greater frication factor and a smaller heat transfer rate were obtained.

Exploring the effective factors on the natural convection over the solid structures assist the researchers to extract a precise and accurate discussion from the obtained data. Lee et al. [21] used a 3D natural convective heat transfer between a cuboidal cavity and a spherical surface. The impacts of Rayleigh numbers and cavity shape parameters were analysed in two different positions of the applied sphere structure including the eccentric and concentric sites. According to the results, a critical Rayleigh number was observed. In this critical point, increment of the temperature difference caused a reduction of the Nusselt number. In another attempt, Kitamura et al. [22] studied natural convection of fluid flow along with water and air heat transfers over a heated sphere structure. Based on the results, the applied flow experienced a turbulent transition. Correlation of average Nusselt number against the Rayleigh numbers were also established for both water and air heat transfer. From literature, it is a common understanding that employing higher thermal conductivity fluid elevates heat transfer performances. Thus, researchers employed nanofluid various applications in their papers [23–36].

Commonly in thermal systems, utilizing an efficient energy is imperative to approach the maximized thermo-dynamic efficiency and estimate the corresponding irreversibility. The performed researches in this area help the engineers to find out the effective methods for reduction of the irreversibility. In this regard, several investigations dealing with the entropy generation have been carried out [37–44].

Several researches have focused on the enclosure cases induced by an inner sphere for evaluation of different boundary conditions. However, the natural convection phenomena and entropy generation of water-based nanofluids around two spheres in a horizontal arrangement have not yet been addressed. So, modelling and analysis of the heat transfer and fluid flow of different nanofluids in the horizontally arranged spheres are of importance which are focused by this study. Then, the effects of nanofluid type (CuO, Cu, and Al_2O_3), volume fraction, coefficient of thermal performance, entropy generation and Rayleigh numbers are investigated numerically on the fluid flow and heat transfer characteristics.

2. Methodology

2.1. Modelling of the system and governing equations

Fig. 1 illustrates main characteristics of the considered problem including the physical domain, coordinate system, and boundary conditions. Herein, two horizontally arranged spheres were kept at a steady and uniform temperature named as T_h. A diameter of D = 0.4 was considered for the applied spheres which were immersed in a channel. The temperature of the upward and downward channel walls was maintained at Tc temperature. A distance of H = 1 was also considered for separation of the channel walls. The inner spheres were placed in the center locations of (xc1, zc1) and (xc2, zc2) with a distance of 0.6 L while L is the length of the horizontal arrangement. The separating distance was filled with nanoflu-

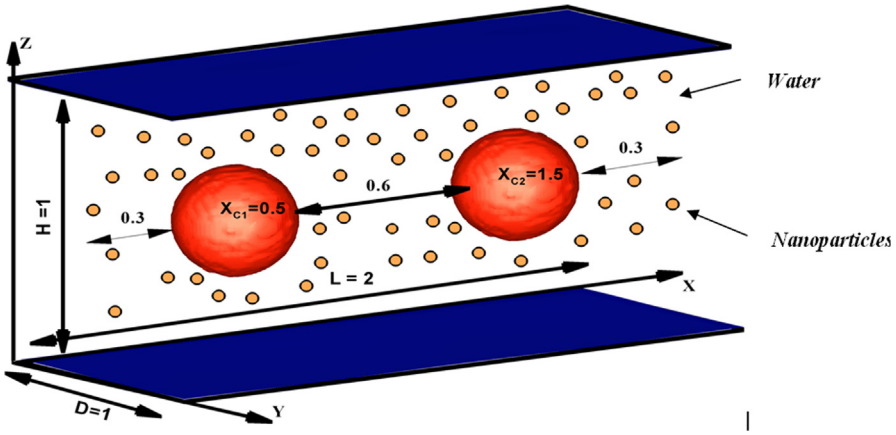

Fig. 1 Schematic description of the physical model.

Table 1 Thermophysical properties of base fluid and nanoparticles.

Property	Water	Al_2O_3	CuO	Cu
ρ (Kg/m^3)	997.1	3970	4250	8933
Cp (J/Kg.K)	4179	765	686.2	385
K (w/m.K)	0.6	40	8.95	401
$\beta \times 10^{-5}$ (1/K)	21	0.85	0.90	1.67

ids of different CuO, Cu, and Al_2O_3 particles with several volume fractions. Thermo physical features of the utilized nanoparticles and water are summarized in Table 1.

In order to define the problem for the system, various items and assumptions were considered consisting acting of the gravity force in the negative direction of the Z-axis, Newtonian feature of the examined fluid, and negligibility of the radiation effects based upon the Boussinesq approximation. Then, the continuity, momentum, and energy-based problem could be defined as follows:

$$\frac{\partial u^*}{\partial x^*}+\frac{\partial v^*}{\partial y^*}+\frac{\partial w^*}{\partial z^*}=0 \tag{1}$$

$$\rho_{nf}\left(\frac{\partial u^*}{\partial t^*}+u^*\frac{\partial u^*}{\partial x^*}+v^*\frac{\partial u^*}{\partial y^*}+w^*\frac{\partial u^*}{\partial z^*}\right) = -\frac{\partial p^*}{\partial x^*}+\mu_{nf}\left(\frac{\partial^2 u^*}{\partial x^{*2}}+\frac{\partial^2 u^*}{\partial y^{*2}}+\frac{\partial^2 u^*}{\partial z^{*2}}\right) \tag{2}$$

$$\rho_{nf}\left(\frac{\partial v^*}{\partial t^*}+u^*\frac{\partial v^*}{\partial x^*}+v^*\frac{\partial v^*}{\partial y^*}+w^*\frac{\partial v^*}{\partial z^*}\right) = -\frac{\partial p^*}{\partial y^*}+\mu_{nf}\left(\frac{\partial^2 v^*}{\partial x^{*2}}+\frac{\partial^2 v^*}{\partial y^{*2}}+\frac{\partial^2 v^*}{\partial z^{*2}}\right) \tag{3}$$

$$\rho_{nf}\left(\frac{\partial w^*}{\partial t^*}+u^*\frac{\partial w^*}{\partial x^*}+v^*\frac{\partial w^*}{\partial y^*}+w^*\frac{\partial w^*}{\partial z^*}\right) = -\frac{\partial p^*}{\partial z^*}+\mu_{nf}\left(\frac{\partial^2 w^*}{\partial x^{*2}}+\frac{\partial^2 w^*}{\partial y^{*2}}+\frac{\partial^2 w^*}{\partial z^{*2}}\right)+\rho_{nf}\beta_{nf}g(T-T_C) \tag{4}$$

$$\rho_{nf}c_{p,nf}\left(\frac{\partial T}{\partial t^*}+u^*\frac{\partial T}{\partial x^*}+v^*\frac{\partial T}{\partial y^*}+w^*\frac{\partial T}{\partial z^*}\right) = k_{nf}\left(\frac{\partial^2 T}{\partial x^{*2}}+\frac{\partial^2 T}{\partial y^{*2}}+\frac{\partial^2 T}{\partial z^{*2}}\right) \tag{5}$$

Table 2 Grid independence test.

Grid size	$\overline{Nu}_{sp}$
80 × 40 × 40	10.771
96 × 48 × 48	11.386
Relative Deviation	(5.401%)
160 × 80 × 80	11.763
Relative Deviation	(3.204%)
180 × 90 × 90	12.177
Relative Deviation	(3.399%)

In order to cast the governing equations into a dimensionless form, the following dimensionless parameters are introduced:

$$\tau=\frac{t^*\alpha_f}{L^2}\,P=\frac{P^*L^2}{\rho_{nf}\alpha_f^2}\,u=\frac{u^*L}{\alpha_f}\,v=\frac{v^*L}{\alpha_f}\,w=\frac{w^*L}{\alpha_f}\,\theta=\frac{T-T_c}{T_h-T_c}$$

$$x=\frac{x^*}{L}\,y=\frac{y^*}{L}\,z=\frac{z^*}{L}$$

Continuity equation:

$$\frac{\partial u}{\partial x}+\frac{\partial v}{\partial y}+\frac{\partial w}{\partial z}=0 \tag{6}$$

Momentum equations:

$$\frac{\partial u}{\partial \tau}+\frac{\partial (uu)}{\partial x}+\frac{\partial (vu)}{\partial y}+\frac{\partial (wu)}{\partial z}=-\frac{\partial p}{\partial x}+\frac{\mu_{nf}}{\alpha_f\rho_{nf}}\left(\frac{\partial^2 u}{\partial x^2}+\frac{\partial^2 u}{\partial y^2}+\frac{\partial^2 u}{\partial z^2}\right) \tag{7}$$

$$\frac{\partial v}{\partial \tau}+\frac{\partial (uv)}{\partial x}+\frac{\partial (uv)}{\partial y}+\frac{\partial (wv)}{\partial z}=-\frac{\partial p}{\partial y}+\frac{\mu_{nf}}{\alpha_f\rho_{nf}}\left(\frac{\partial^2 v}{\partial x^2}+\frac{\partial^2 v}{\partial y^2}+\frac{\partial^2 v}{\partial z^2}\right) \tag{8}$$

$$\frac{\partial w}{\partial \tau}+\frac{\partial (uw)}{\partial x}+\frac{\partial (vw)}{\partial y}+\frac{\partial (ww)}{\partial z}=-\frac{\partial p}{\partial z}+\frac{\mu_{nf}}{\alpha_f\rho_{nf}}\left(\frac{\partial^2 w}{\partial x^2}+\frac{\partial^2 w}{\partial y^2}+\frac{\partial^2 w}{\partial z^2}\right)+\frac{(\rho\beta)_{nf}}{\rho_{nf}\beta_f}Ra\Pr\theta \tag{9}$$

Energy Equation:

$$\frac{\partial \theta}{\partial \tau}+\frac{\partial (u\theta)}{\partial x}+\frac{\partial (v\theta)}{\partial y}+\frac{\partial (w\theta)}{\partial z}=\frac{\alpha_{nf}}{\alpha_f}\left(\frac{\partial^2 \theta}{\partial x^2}+\frac{\partial^2 \theta}{\partial y^2}+\frac{\partial^2 \theta}{\partial z^2}\right) \tag{10}$$

The boundary conditions, in the present study, are as follows:

- u=v=w=0 on all walls
- $\left.\frac{\partial\theta}{\partial z}\right|_{z=0}=\left.\frac{\partial\theta}{\partial z}\right|_{z=1}=0$ at 0≤x,y≤1
- θ=0 at 0≤x,0, z≤1 , 0≤x,1,z≤1 , 0≤0,y,z≤1 and 0≤1,y,z≤1
- θ=1 on the surface of inner sphere

The Rayleigh number and Prandtl number are defined as: $Ra=\frac{g\beta_f(T_h-T_c)L^3}{\alpha_f\nu_f}$ and $\Pr=\frac{\nu_f}{\alpha_f}$

Table 3 Comparison of average Nusselt number values obtained for the flow in the presence of isothermal hot sphere centrally located within a cubical enclosure, with those obtained from the previous numerical studies.

Ra	Present work (Grid size 80^3)	Yoon et al. [69]	Gulberg & Feldman [70]
10^3	6.429	7.575	–
10^4	7.368	7.859	8.314
10^5	12.093	12.658	13.415
10^6	19.759	20.701	22.344

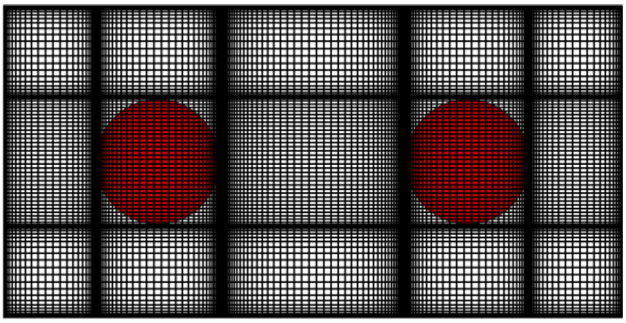

Fig. 2 Mesh configuration of computational domain (size 160 × 80 × 80).

So as to solve mathematically Navier-Stokes conditions, authors followed the following strategy;

The temporal discretization of the time derivative is performed by a Euler backward second-order implicit scheme. The strong velocity–pressure coupling present in the continuity and the momentum equations is handled by implementing the projection method [45]. The QUICK scheme of Hayase et al. [46] is implemented to minimize the numerical diffusion for the advective terms. The Poisson equation which is solved using an accelerated full multigrid method, while the discretized equations are computed using the red and black point successive over-relaxation method [47] with the choice of optimum relaxation factors. In order to secure the steady state conditions, the following criterion has to be satisfied:

$$\sum_{i,j,k}\left|\chi^{n}_{i,j,k}-\chi^{n-1}_{i,j,k}\right|\leqslant 10^{-6}$$

where n represents the iteration number. In addition, i, j, and k indicate x, y, and z coordinates, respectively.

An in-house code was created in the well-known programming language of FORTRAN to complete the calculations. For doing the accurate calculations, the applied programming language was depended on several methods consisting of the projection technique, finite volume method (FVM), and multigrid acceleration [48–54]. The terms of Nu and $\bar{Nu}$, respectively, known as the local and average values of the Nusselt numbers which could be defined through the following equation:

$$Nu=\left.\frac{\partial\theta}{\partial n}\right|_{wall},\ \bar{Nu}=\frac{1}{A}\int_{0}^{A}NudS \tag{11}$$

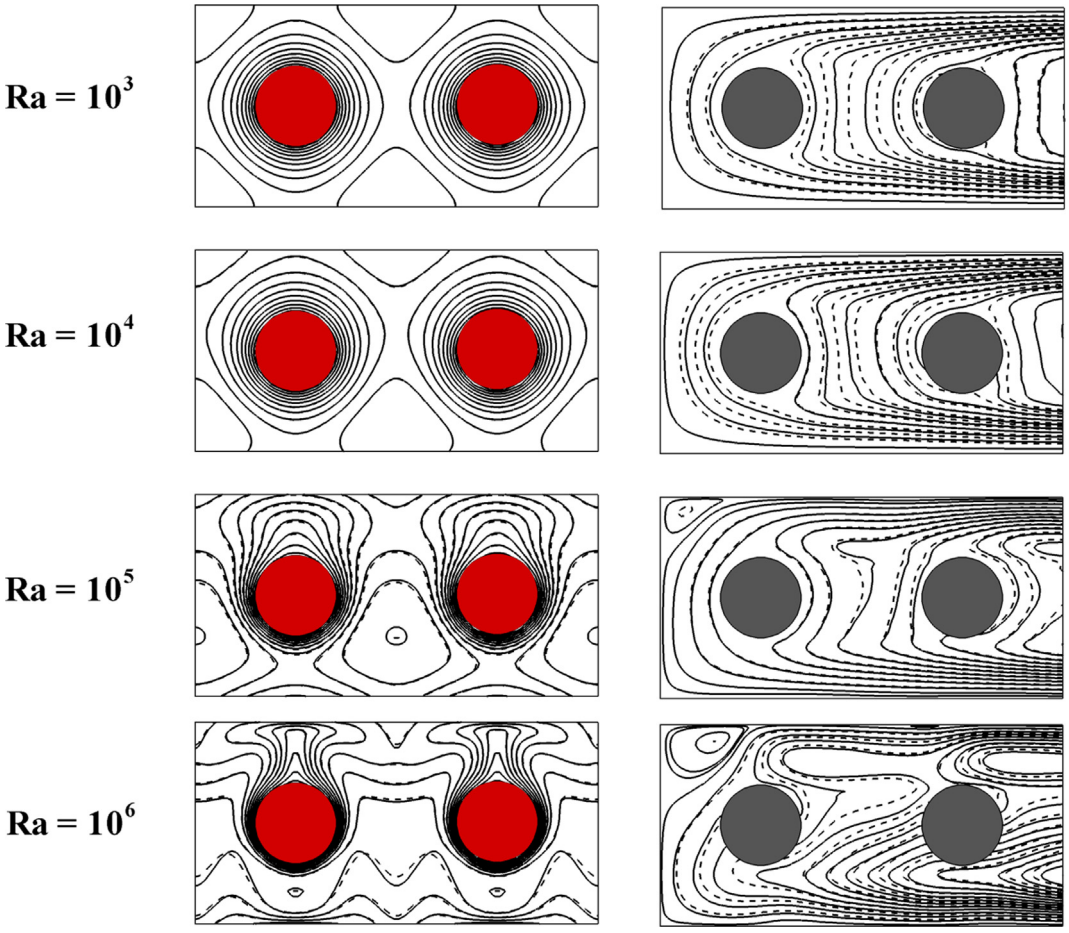

Fig. 3 Isocontours of isotherms (on the left) and streamlines (on the right) of pure water $\phi = 0$ (solid lines) and CuO-water nanofluid with volume fraction of nanoparticles $\phi = 0.08$ (dashed lines) at the vertical plane (y, z) for Rayleigh numbers ranging from 10^3 to 10^6.

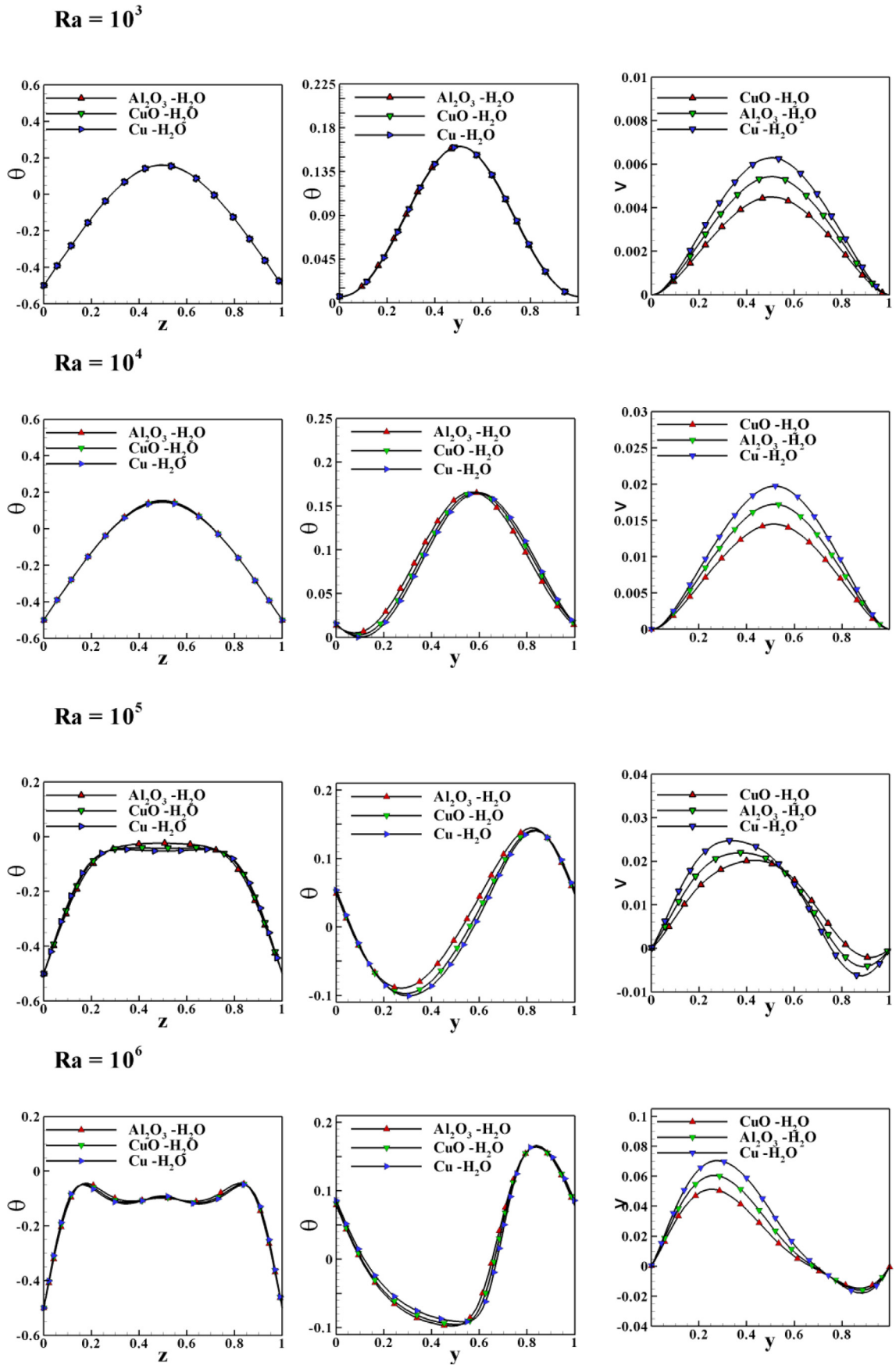

Fig. 4 Variation of the temperature θ versus z, θ versus y and the velocity v versus y of CuO-water, Cu-water and Al_2O_3-water nanofluid with volume fraction of nanoparticles $\phi = 0.08$ at the vertical plane (y, z) for Rayleigh numbers ranging from 10^3 to 10^6.

Table 4 The maximal and minimal temperature values ($\theta_{y,max}$ and $\theta_{y,min}$) for different nanofluids at different Rayleigh numbers and solid volume fractions.

	10^3		10^4		10^5		10^6	
	$\theta_{y,min}$	$\theta_{y,max}$	$\theta_{y,min}$	$\theta_{y,max}$	$\theta_{y,min}$	$\theta_{y,max}$	$\theta_{y,min}$	$\theta_{y,max}$
φ = 2%								
Al_2O_3-H_2O	0.0074	0.16206	0.0021	0.16590	−0.0976	0.14310	−0.1008	0.16163
Cu-H_2O	0.0074	0.16207	0.0004	0.16556	−0.1004	0.14238	−0.1005	0.16060
CuO-H_2O	0.0074	0.16210	0.0011	0.16569	−0.0993	0.14263	−0.1013	0.16044
φ = 4%								
Al_2O_3-H_2O	0.0071	0.16164	0.0032	0.16588	−0.0953	0.14325	−0.0994	0.16279
Cu-H_2O	0.0071	0.16168	0.0021	0.14538	−0.1007	0.14182	−0.0974	0.16246
CuO-H_2O	0.0072	0.16174	0.0014	0.16565	−0.0988	0.14227	−0.0991	0.16196
φ = 6%								
Al_2O_3-H_2O	0.0068	0.16122	0.0043	0.16596	−0.0925	0.14380	−0.0982	0.16367
Cu-H_2O	0.0068	0.16127	0.0021	0.14545	−0.1007	0.14125	−0.0943	0.16441
CuO-H_2O	0.0069	0.16136	0.0018	0.16565	−0.0980	0.14202	−0.0971	0.16344
φ = 8%								
Al_2O_3-H_2O	0.0065	0.16078	0.0050	0.16587	−0.0892	0.14490	−0.0974	0.16423
Cu-H_2O	0.0065	0.16084	0.0021	0.14594	−0.1004	0.14074	−0.0914	0.16631
CuO-H_2O	0.0066	0.16097	0.0023	0.16554	−0.0971	0.14170	−0.0953	0.16481

Table 5 The maximal and minimal temperature values ($\theta_{z,max}$ and $\theta_{z,min}$) for different nanofluids at different Rayleigh numbers and solid volume fractions.

	10^3		10^4		10^5		10^6	
	$\theta_{Z,min}$	$\theta_{Z,max}$	$\theta_{Z,min}$	$\theta_{Z,max}$	$\theta_{Z,min}$	$\theta_{Z,max}$	$\theta_{Z,min}$	$\theta_{Z,max}$
φ = 2%								
Al_2O_3-H_2O	−0.5	0.16197	−0.5	0.14922	−0.5	−0.04151	−0.5	−0.04458
Cu-H_2O	−0.5	0.16191	−0.5	0.14585	−0.5	−0.04499	−0.5	−0.04688
CuO-H_2O	−0.5	0.16197	−0.5	0.14734	−0.5	−0.04383	−0.5	−0.04630
φ = 4%								
Al_2O_3-H_2O	−0.5	0.16161	−0.5	0.15135	−0.5	−0.03730	−0.5	−0.04469
Cu-H_2O	−0.5	0.16151	−0.5	0.14538	−0.5	−0.04559	−0.5	−0.04770
CuO-H_2O	−0.5	0.16162	−0.5	0.14800	−0.5	−0.04340	−0.5	−0.04660
φ = 6%								
Al_2O_3-H_2O	−0.5	0.16123	−0.5	0.15326	−0.5	−0.03080	−0.5	−0.04493
Cu-H_2O	−0.5	0.16111	−0.5	0.14545	−0.5	−0.04587	−0.5	−0.04832
CuO-H_2O	−0.5	0.16127	−0.5	0.14890	−0.5	−0.04230	−0.5	−0.04681
φ = 8%								
Al_2O_3-H_2O	−0.5	0.16084	−0.5	0.15496	−0.5	−0.02353	−0.5	−0.04423
Cu-H_2O	−0.5	0.16070	−0.5	0.14594	−0.5	−0.04583	−0.5	−0.04875
CuO-H_2O	−0.5	0.16091	−0.5	0.14995	−0.5	−0.04069	−0.5	−0.04697

where n and A are corresponded to the normal direction and solid sphere surface area, respectively. More details of the applied mathematical calculations could be found in the study carried out by Ben-Cheikh et al. [48].

2.2. Thermo physical characteristics of the utilized nanofluids

Effective density as well as specific heat capacity, shown by ρ_{nf} and *Cp*, are of the main thermophysical nanofluid features. The following functions reveal the relations applied for calculation of the aforementioned parameters:

Nanofluid density [55]

$$\rho_{nf} = \phi\rho_p + (1-\phi)\rho_f \tag{12}$$

Nanofluid specific heat capacity [56]

$$(\rho C_p)_{nf} = (1-\phi)(\rho C_p)_f + \phi(\rho C_p)_p \tag{13}$$

Thermal conductivity [57]

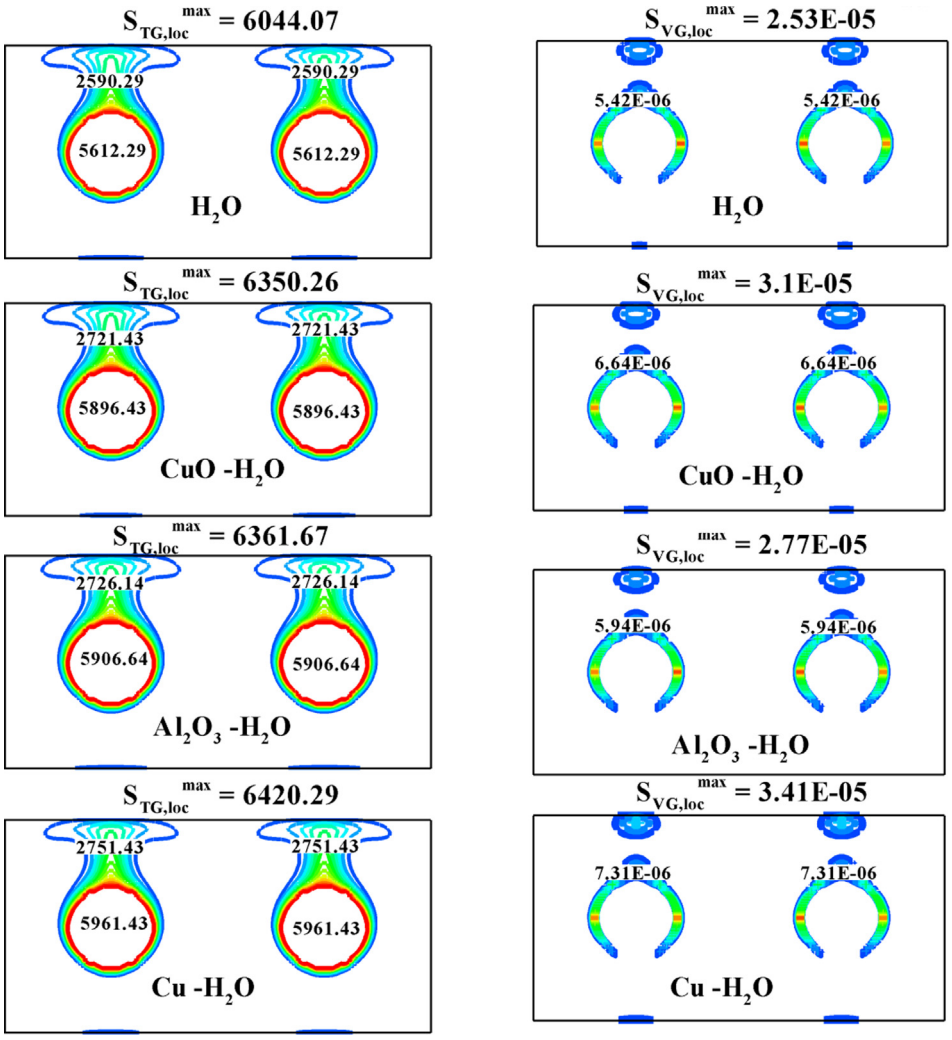

Fig. 5 Isosurfaces of maximum local entropy generation contours due to heat transfer $S^{max}_{TG,loc}$ (on the left) and due to fluid friction $S_{VG,loc}{}^{max}$ (on the right) of pure water $\phi = 0$ and different nanofluids (CuO-water, Al_2O_3-water and Cu-water) with volume fraction of nanoparticles $\phi = 0.08$ at the vertical plane (y, z) for $Ra = 10^6$.

$$k_{nf} = \frac{k_p + (n-1)k_f - (n-1)(k_f - k_p)\phi}{k_p + (n-1)k_f + (k_f - k_p)\phi} k_f \tag{14}$$

Here, n is equal to $(=\frac{3}{\varphi})$ and is linked with the empirical shape factor. In addition, φ reveals sphericity which could be estimated through the surface area ratio of the applied sphere to the utilized particles. For the spherical and cylindrical shape cases, the sphericity value is equal to 1 and 0.5, respectively.

So, according to spherical nanoparticles k_{nf} is given by Maxwell [58]:

$$k_{nf} = \frac{(k_p + 2k_f) - 2\phi(k_f - k_p)}{(k_p + 2k_f) + \phi(k_f - k_p)} k_f \tag{15}$$

Dynamic viscosity [59]

$$\mu_{nf} = \frac{\mu_f}{(1-\phi)^{2.5}} \tag{16}$$

Thermal expansion coefficient [60]

$$\beta_{nf} = \left[\frac{\beta_p}{\left(1 + \frac{(1-\phi)\rho_f}{\phi\rho_p}\right)} + \frac{1}{1 + \frac{\phi\rho_p}{(1-\phi)\rho_f}} \right] \beta_f \tag{17}$$

And

$$\alpha_{nf} = \frac{k_{nf}}{(\rho C_p)_{nf}} \tag{18}$$

In the previous expressions, subscripts f and p are pertaining to pure fluid and dispersed nanoparticles, respectively. The calculated features of the CuO, Cu, and Al_2O_3 nanoparticles as well as the base fluid used in the study are detailed in Table 1.

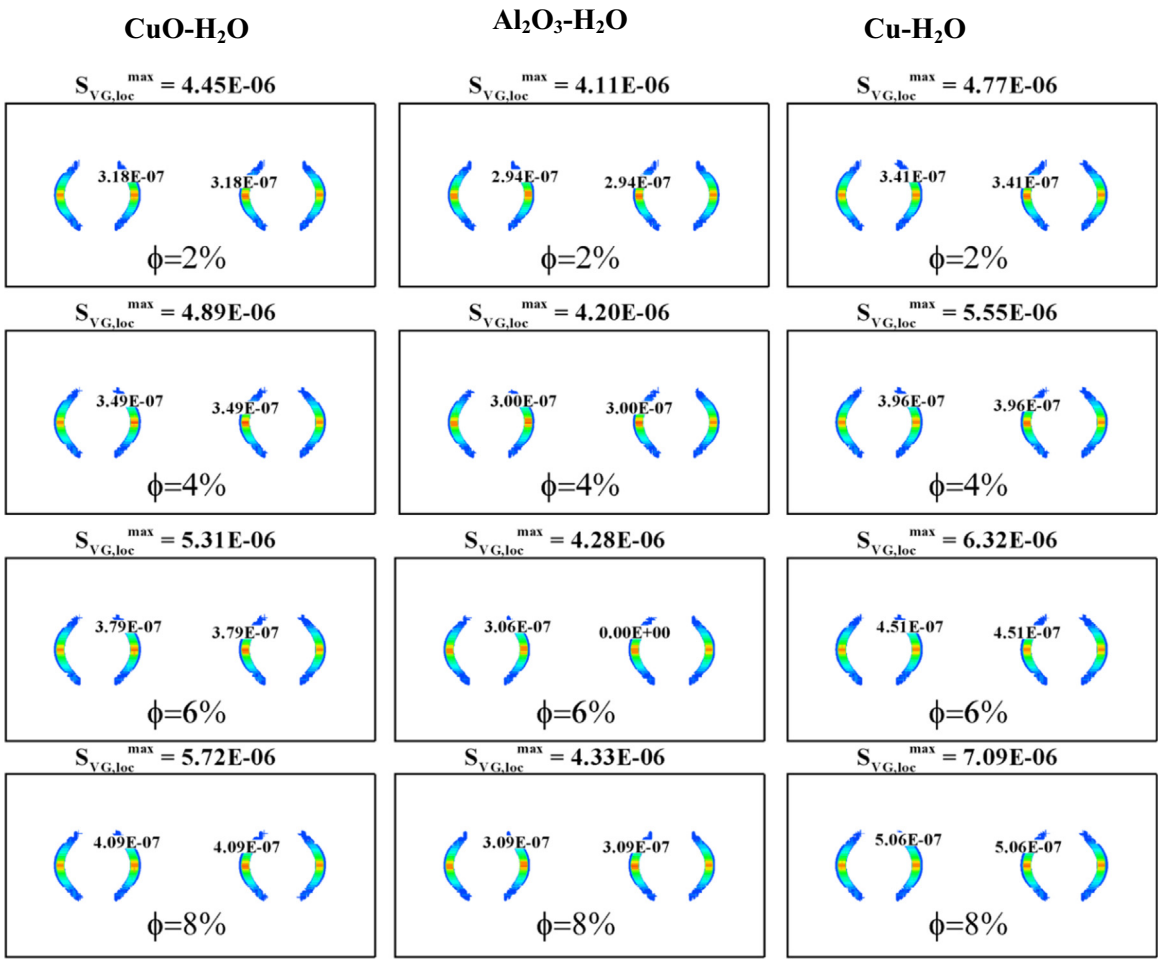

Fig. 6 Isosurfaces of maximum local entropy generation contours due to friction $S_{VG,loc}^{max}$ of different nanofluids (CuO-water, Al_2O_3-water and Cu-water) with various volume fraction of nanoparticles (ϕ = 0.02, 0.04, 0.06 and 0.08) at the vertical plane (y, z) for Ra = 10^4.

2.3. Entropy generation functions

Numerous researches have reported the entropy generation theory [61–67]. Heat transfer along with fluid friction are defined as irreversibility in the case of three-dimensional convective heat transfer problems. Eq. (19) represents the general function explaining the entropy generation in the considered specific system:

$$S_{gen}^{*} = -\frac{1}{T_0^2}.\vec{q}.\vec{\nabla}T + \frac{\mu}{T_0}.\Phi^{*} \tag{19}$$

In the equation above, two terms are observable. The first one is assigned to the generated entropy as a result of gradient in the temperature. Whilst, the second one is attributed to the friction effects. The irreversibility coefficient ($\vec{q}$) could be obtained by using the Eq. (20):

$$\vec{q} = -k.gra\vec{d}\,T \tag{20}$$

The dissipation function is written in incompressible flow as follows:

$$\Phi^{*} = 2\left[\left(\frac{\partial u^{*}}{\partial x^{*}}\right)^{2} + \left(\frac{\partial v^{*}}{\partial y^{*}}\right)^{2} + \left(\frac{\partial w^{*}}{\partial z^{*}}\right)^{2}\right] + \left(\frac{\partial v^{*}}{\partial x^{*}} + \frac{\partial u^{*}}{\partial y^{*}}\right)^{2} + \left(\frac{\partial w^{*}}{\partial y^{*}} + \frac{\partial v^{*}}{\partial z^{*}}\right)^{2} + \left(\frac{\partial u^{*}}{\partial z^{*}} + \frac{\partial w^{*}}{\partial x^{*}}\right)^{2} \tag{21}$$

From where the generated entropy [68] is written as

$$S_{gen}^{*} = \frac{k}{T_0^2}\left[\left(\frac{\partial T}{\partial x^{*}}\right)^{2} + \left(\frac{\partial T}{\partial y^{*}}\right)^{2} + \left(\frac{\partial T}{\partial z^{*}}\right)^{2}\right] + 2\frac{\mu_0}{T_0}\left\{\left[\left(\frac{\partial u^{*}}{\partial x^{*}}\right)^{2} + \left(\frac{\partial v^{*}}{\partial y^{*}}\right)^{2} + \left(\frac{\partial w^{*}}{\partial z^{*}}\right)^{2}\right] + \left(\frac{\partial v^{*}}{\partial x^{*}} + \frac{\partial u^{*}}{\partial y^{*}}\right)^{2} + \left(\frac{\partial w^{*}}{\partial y^{*}} + \frac{\partial v^{*}}{\partial z^{*}}\right)^{2} + \left(\frac{\partial u^{*}}{\partial z^{*}} + \frac{\partial w^{*}}{\partial x^{*}}\right)^{2}\right\} \tag{22}$$

After non-dimensionalization, the generated entropy number (dimensionless local entropy generated) is written in the following way as

$$N_s = S_{gen}^{*}\frac{1}{k}\left(\frac{LT_0}{\Delta T}\right)^{2} \tag{23}$$

From where [68]

$$N_s = \left[\left(\frac{\partial \theta}{\partial x}\right)^{2} + \left(\frac{\partial \theta}{\partial y}\right)^{2} + \left(\frac{\partial \theta}{\partial z}\right)^{2}\right] + \varphi.\left\{2\left[\left(\frac{\partial u}{\partial x}\right)^{2} + \left(\frac{\partial v}{\partial y}\right)^{2} + \left(\frac{\partial w}{\partial z}\right)^{2}\right] + \left(\frac{\partial v}{\partial x} + \frac{\partial u}{\partial y}\right)^{2} + \left(\frac{\partial w}{\partial y} + \frac{\partial v}{\partial z}\right)^{2} + \left(\frac{\partial u}{\partial z} + \frac{\partial w}{\partial x}\right)^{2}\right\} \tag{24}$$

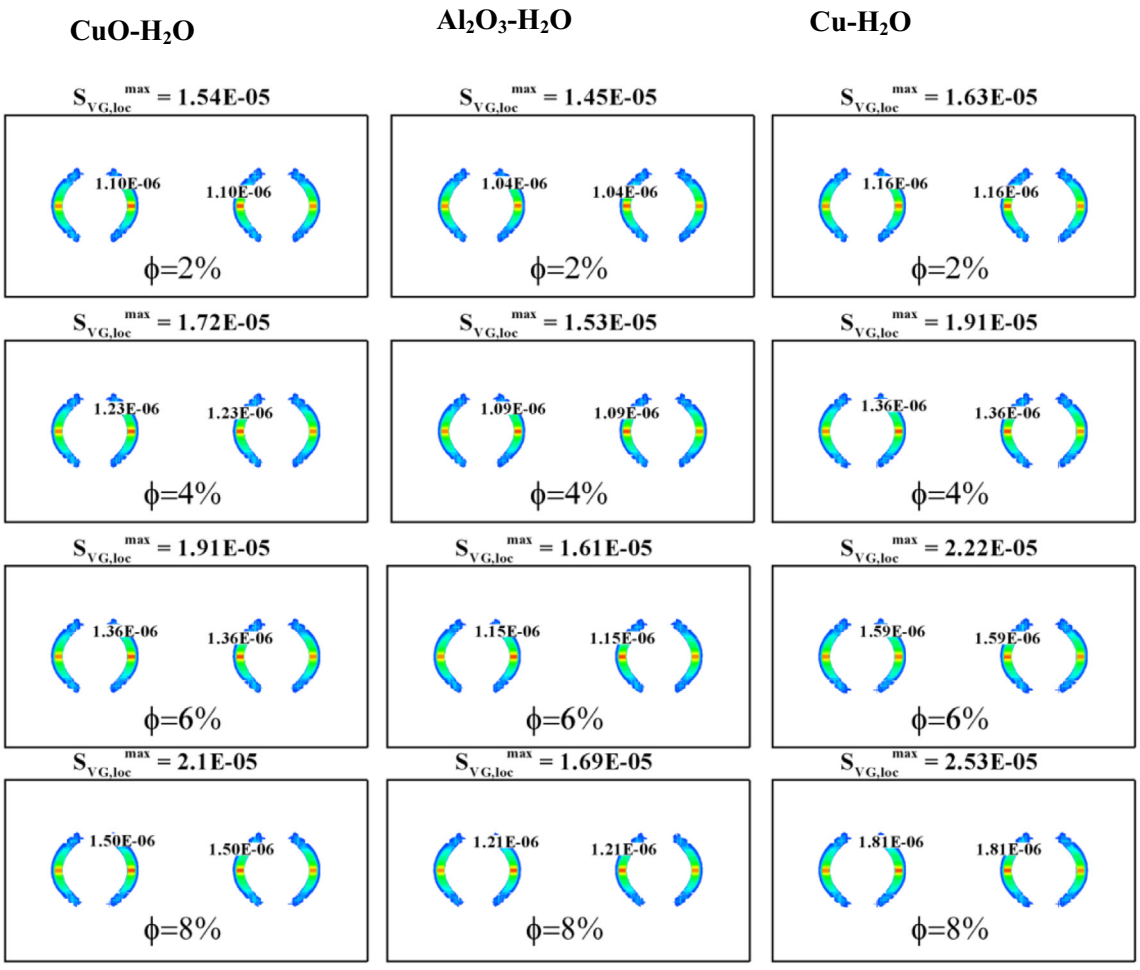

Fig. 7 Isosurfaces of maximum local entropy generation contours due to friction $S^{max}_{VG,loc}$ of different nanofluids (CuO-water, Al_2O_3-water and Cu-water) with various volume fraction of nanoparticles (ϕ = 0.02, 0.04, 0.06 and 0.08) at the vertical plane (y, z) for Ra = 10^5.

The total dimensionless generated entropy is written as follows:

$$S^{loc}_{tot} = \int_0^1 \int_0^1 \int_0^1 N_s d_v = \int_0^1 \int_0^1 \int_0^1 (N_{s-TG} + N_{s-VG}) d_v = S^{loc}_{TG} + S^{loc}_{VG} \quad (25)$$

Bejan number (Be) is the ratio of heat transfer irreversibility to the total irreversibility due to heat transfer and fluid friction.

$$Be = \frac{S_{TG}}{S_{TG} + S_{VG}} \quad (26)$$

where

$$S^{loc}_{T} = S^{loc}_{TG} + S^{loc}_{VG} \quad (27)$$

$$S^{loc}_{TG} = \left[\left(\frac{\partial \theta}{\partial x}\right)^2 + \left(\frac{\partial \theta}{\partial y}\right)^2 + \left(\frac{\partial \theta}{\partial z}\right)^2 \right] \quad (28)$$

$$S^{loc}_{VG} = \varphi \left[2\left(\frac{\partial u}{\partial x}\right)^2 + 2\left(\frac{\partial u}{\partial y}\right)^2 + 2\left(\frac{\partial u}{\partial z}\right)^2 + \left(\frac{\partial v}{\partial x} + \frac{\partial u}{\partial y}\right)^2 + \left(\frac{\partial w}{\partial y} + \frac{\partial v}{\partial z}\right)^2 + \left(\frac{\partial u}{\partial z} + \frac{\partial w}{\partial x}\right)^2 \right] \quad (29)$$

With

$$\varphi = \frac{\mu T_0}{k} \left(\frac{u_0}{\Delta T}\right)^2 \quad (30)$$

Is the irreversibility coefficient.

The dimensionless total entropy generation S_{tot} in the enclosure is given by the summation of the total entropy generation due to heat transfer S_{TG} and fluid friction S_{VG} which in turn are obtained via integrating the local entropy generation rates $S_{TG,loc}$ and $S_{VG,loc}$ over the domain Ω:

The total entropy generation (S_{tot}) is a dimensionless term. It could be obtained through the equation (31):

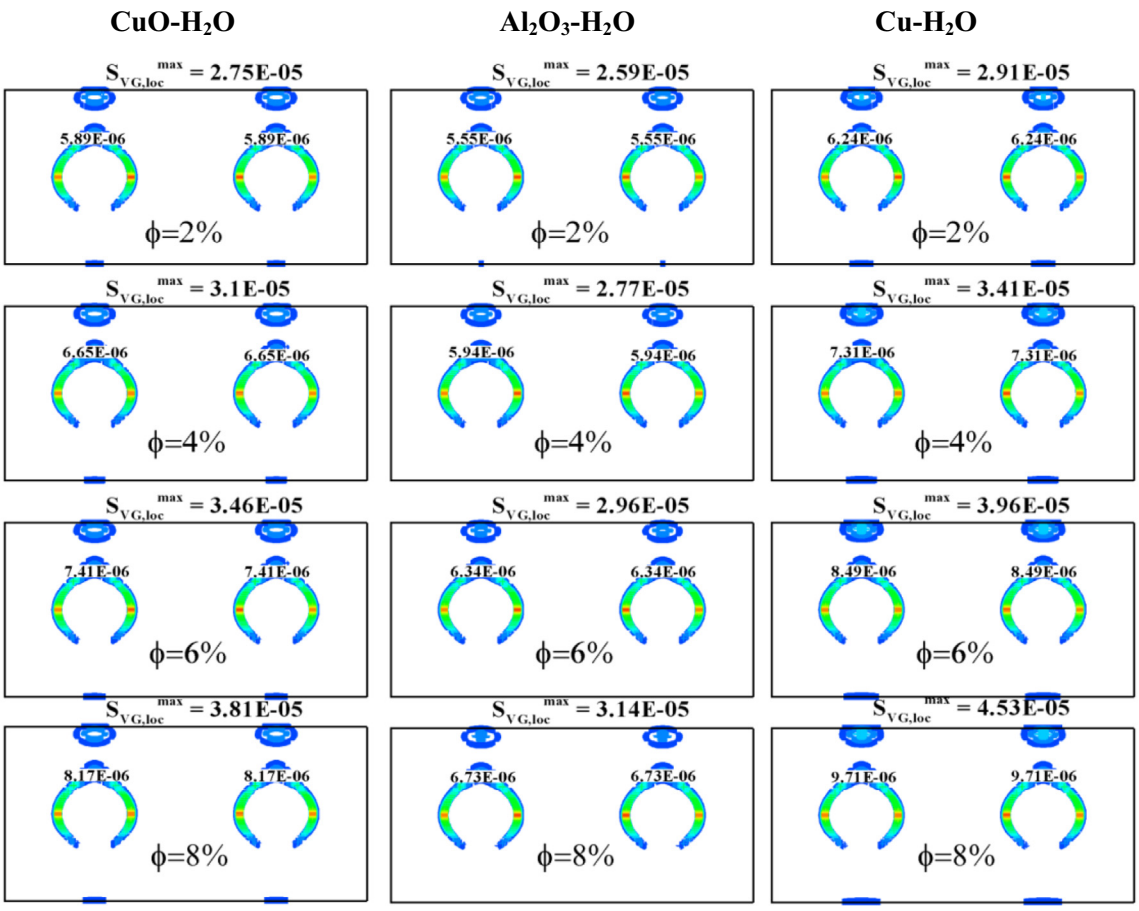

Fig. 8 Isosurfaces of maximum local entropy generation contours due to friction $S^{max}_{VG,loc}$ of different nanofluids (CuO-water, Al_2O_3-water and Cu-water) with various volume fraction of nanoparticles (ϕ = 0.02, 0.04, 0.06 and 0.08) at the vertical plane (y, z) for Ra = 10^6.

$$S_{tot} = \int_{\Omega} S^{loc} d\Omega = \int_{\Omega} S^{loc}_{TG} d\Omega + \int_{\Omega} S^{loc}_{VG} d\Omega = S_{TG} + S_{VG} \qquad (31)$$

where S_{TG} and S_{VG} are corresponded to the generated entropy by heat transfer and fluid friction, respectively. As shown in the equation, both parameters could be calculated through integration of the local generated entropies over the considered domain (Ω).

3. Grid independence study and algorithm validation

3.1. Grid independence evaluation

The grid independence examination was performed through considering the values of Pr = 7.02 (base fluid-water) and Ra = 10^3, respectively. Four different non-uniform grids including 80 × 40 × 40, 96 × 48 × 48, 160 × 80 × 80, and 180 × 90 × 90 was employed to simulate the convective heat transfer over two isothermal solid spheres located in a cooled channel. The average Nusselt numbers calculated from the spheres are listed in Table 2. To consider a problem solution independent from the applied grid, the fine and non-uniform grid of 160 × 80 × 80 was utilized.

3.2. Code validation

Numerical simulations were performed and compared with those reported by Yoon et al. [69] and Gulberg and Feldman [70]. As explained, the code validation was carried out for the three-dimensional natural convection problem. The applied isothermal solid sphere was centrally located in a cooled outer one. The estimated average values of the Nusselt numbers along with the reported values by Yoon et al. [69] and Gulberg and Feldman [70] are listed in Table 3. The Nusselt number values are all obtained for different Rayleigh numbers in the range from 10^3 to 10^6 in center of the inner sphere. As it is apparent from the table, the obtained values are in well agreement with the ones obtained through the aforementioned researches (see Fig. 2).

4. Results and discussion

4.1. Flow and thermal fields

In this study, convective heat transfer and entropy generation around two spheres in a horizontal arrangement filled with

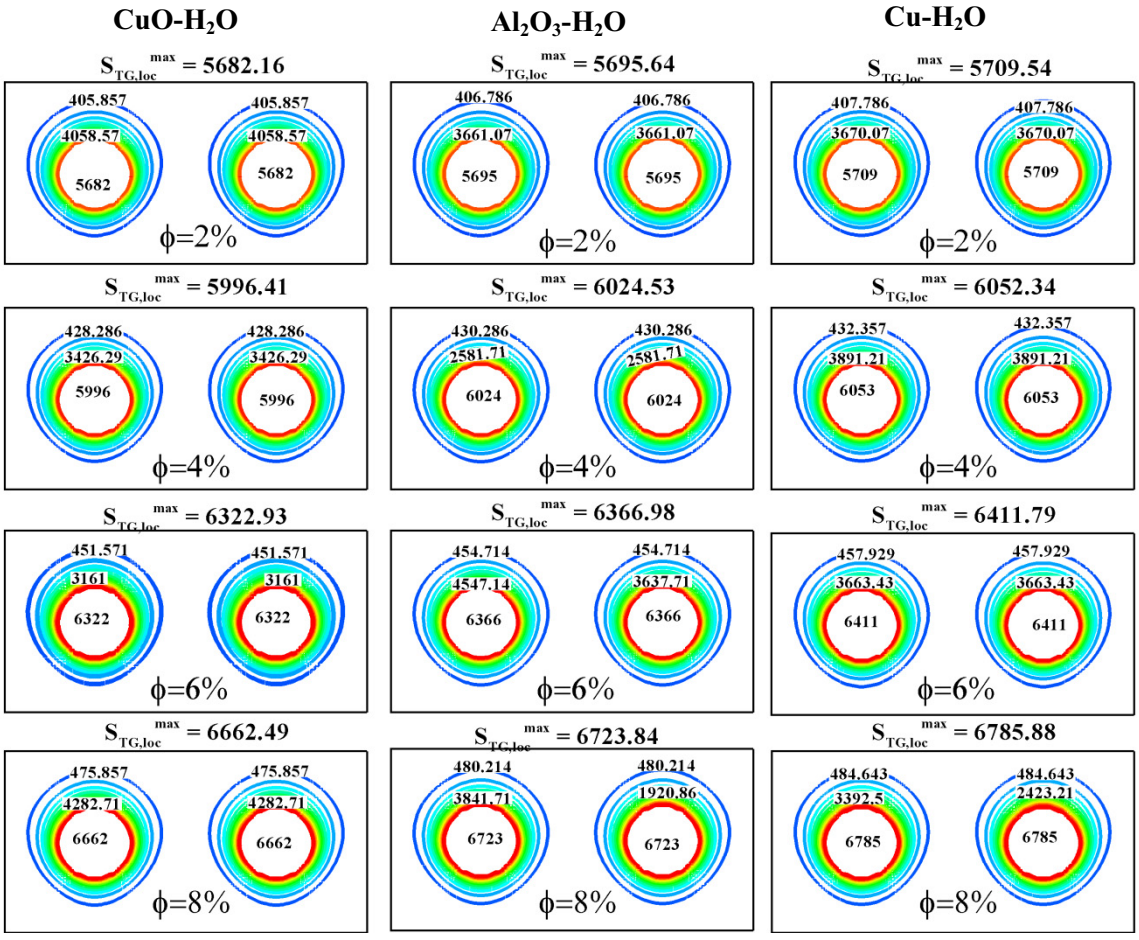

Fig. 9 Isosurfaces of maximum local entropy generation contours due to heat transfer $S^{max}_{TG,loc}$ of different nanofluids (CuO-water, Al_2O_3-water and Cu-water) with various volume fraction of nanoparticles (ϕ = 0.02, 0.04, 0.06 and 0.08) at the vertical plane (y, z) for Ra = 10^4.

water-based nanofluids (CuO-water, Cu-water and Al_2O_3-water) are investigated numerically using FVM. The different thermo-physical characteristics of based fluid and different nanoparticles are shown in Table 1 as already mentioned. Calculations are made for various values of the volume fraction of nanoparticles (ϕ = 0%, 2%, 4%, 6% and 8%), for different values of Rayleigh numbers (Ra = 10^3, 10^4, 10^5 and 10^6). The Prandtl number of the base fluid (pure water) is kept constant at 7.02. To demonstrate qualitatively the effect of different Rayleigh numbers and nanoparticle types on the temperature and fluid flow distributions of two side-by-side spheres, Fig. 3 shows the Isocontours of isotherms (left) and streamlines (right) of pure water ϕ = 0 (solid lines) and CuO-water nanofluid with volume fraction of nanoparticles ϕ = 0.08 (dashed lines) at the vertical plane (y, z) for Rayleigh numbers ranging from 10^3 to 10^6. It may be seen from this figure that the temperature contours consist of two counter rotating cells for Rayleigh numbers 10^3 and 10^4. In fact, the buoyant forces generated due to the fluid temperature differences cause the fluid to rise on the sides and to descend in the middle of the enclosure. This movement of the fluid forms counters rotating circulating cells within the enclosure exhibit a perfect symmetric behaviour about the cavity mid plane; this fact is due to the symmetry of both spheres about the mid plane. As the Rayleigh number equates 10^5 and 10^6, the buoyancy force ascends overcoming the viscous force; thus, heat transfer is dominated by convection. It is observed that compression at the level of the spheres due to the stronger convection effects. Likewise, a thermal plume appears in the upper part of both spheres.

The corresponding streamlines displayed in the right part of Fig. 3 present a mono-cellular flow for the Rayleigh numbers valued in the range from 10^3 to 10^6. Based on the figure, at the vicinity region of the applied spheres, large streamlines were obtained. While, close to the horizontal walls a stratified core phase has been appeared. When the Rayleigh number was equal to 10^6, reduction of streamlines was apparently observed especially in the centreline. However, it was stratified slightly in both upper and lower plates of the arrangement. The observed distortion in the centreline could be linked with the considered highest value for the Rayleigh number and therefore domination of the convection. In order to compare the obtained data, the results of the pure water were also provided in the figure. Apparently, the flow field strength was reduced by introduction of the nanoparticles into the pure water. In addition, as nanoparticles are added, the maximum dimensionless temperature is reduced which is an indication of enhancing the enclosure cooling performance.

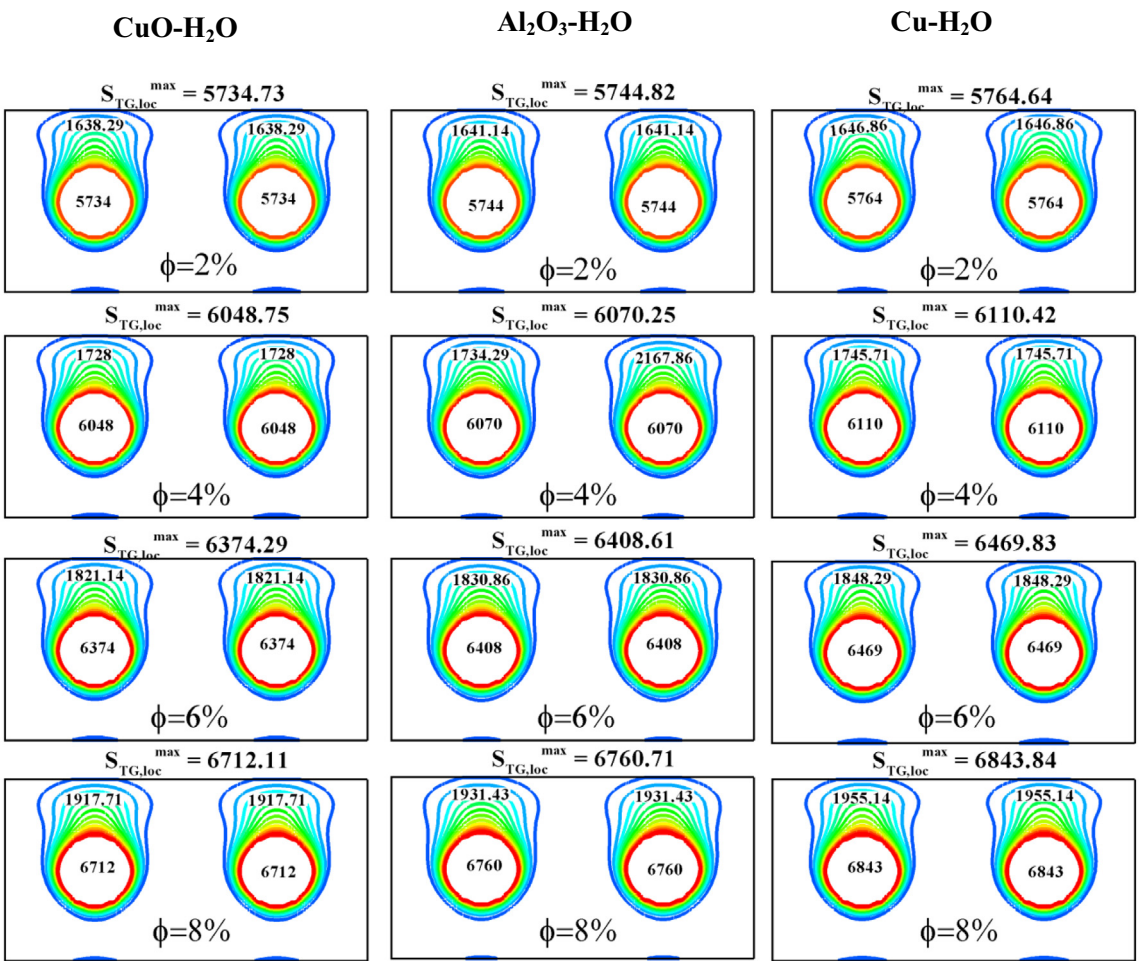

Fig. 10 Isosurfaces of maximum local entropy generation contours due to heat transfer $S_{TG,loc}^{max}$ of different nanofluids (CuO-water, Al_2O_3-water and Cu-water) with various volume fraction of nanoparticles (ϕ = 0.02, 0.04, 0.06 and 0.08) at the vertical plane (y, z) for Ra = 10^5.

Fig. 4 explains the combined correlation between the results obtained through incorporation of the Cu, Al_2O_3, and CuO nanoparticles into the pure water for the temperature versus z and y and the velocity, respectively. Volume fraction of the nanoparticles was considered as ϕ = 0.08 for the measurement. In addition, the Rayleigh numbers varied in the range from 10^3 to 10^6. Notably, the temperature profiles (θ) against the z axis were almost confusing for all Rayleigh numbers. However, it showed a very slight variation against the y axis. According to the results, it was remarked that Al_2O_3 had a higher temperature compared with both CuO and Cu nanoparticles. Based on the velocity profiles, it was also found that the velocity of Cu was higher than that of the Al_2O_3 nanoparticles. While, CuO nanoparticles showed the lowest velocity in the considered Rayleigh numbers. The observed trend was exhibited as a result of higher thermal conductivity value of Cu as shown in Table 1.

At this stage, in order to show the effects of the addition of nanoparticles on maximal and minimal temperatures, Tables 4 and 5 display the temperature values along y and z for the horizontal arrangement incorporating two spheres for different nanofluids, Rayleigh numbers and solid volume fractions. As mentioned earlier, these two cases show the sensitivity of temperature values to the volume fraction of nanoparticles which is related to the increased thermal conductivity of the nanofluid. Indeed, higher values of thermal conductivity are accompanied by higher values of thermal diffusivity. The high value of thermal diffusivity causes a drop in the temperature gradients and accordingly increases the temperature values.

4.2. Entropy generation analysis

Fig. 5 illustrates the maximum local distribution of the entropy generation contours resulting from irreversibility of the heat transfer STG, locmax (left) as well as the fluid friction SVG, locmax (right) within the horizontal arrangement. The entropy generation was provided for pure water (ϕ = 0) and different nanofluids (CuO-water, Al_2O_3-water and Cu-water) with a constant volume fraction of ϕ = 0.08 at the vertical plane (y, z). The value of 10^6 was also considered for the Rayleigh number. STG active phase has occurred at the spheres' core representing the STG local distribution resulting from the heat transfer between the spheres and the horizontal arrangement. As the entropy maps are represented for the water, CuO,

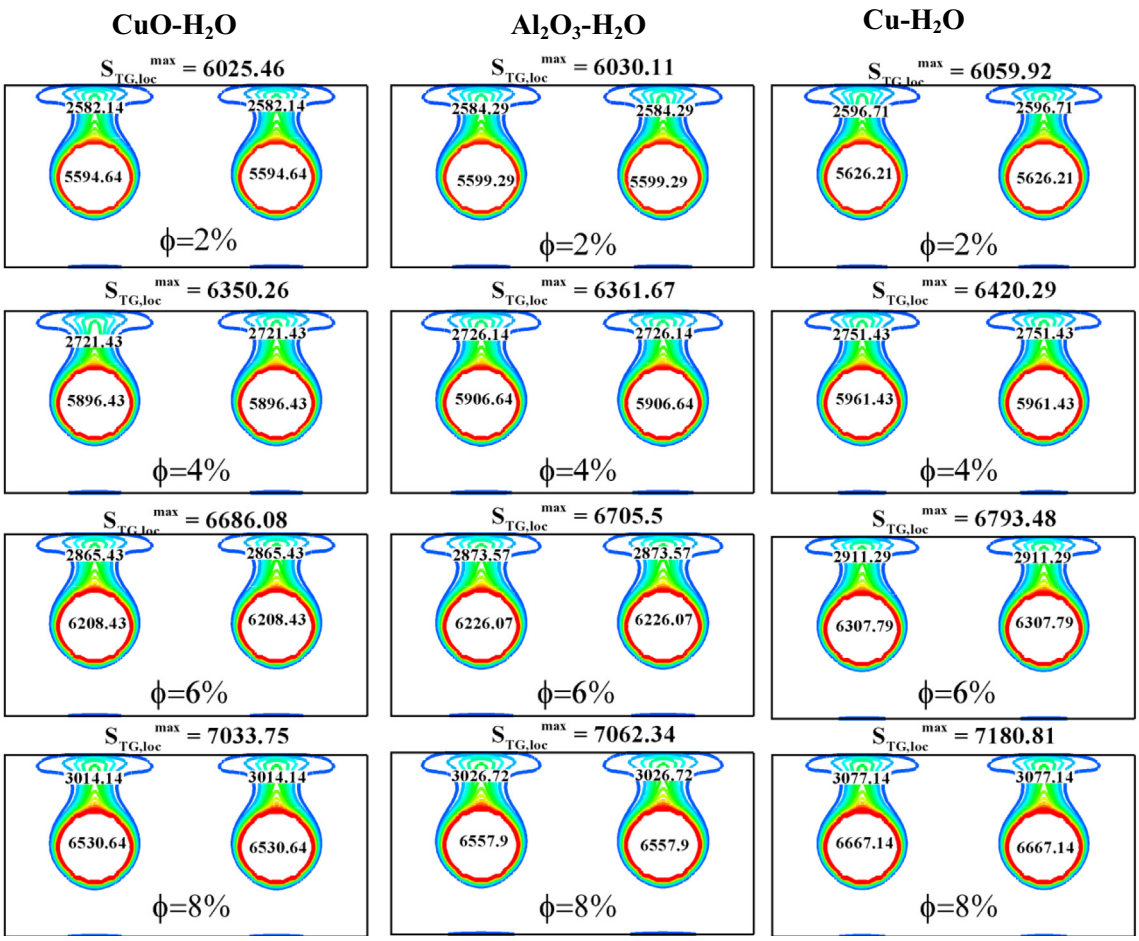

Fig. 11 Isosurfaces of maximum local entropy generation contours due to heat transfer $S^{max}_{TG,loc}$ of different nanofluids (CuO-water, Al_2O_3-water and Cu-water) with various volume fraction of nanoparticles (ϕ = 0.02, 0.04, 0.06 and 0.08) at the vertical plane (y, z) for Ra = 10^6.

Al_2O_3, and Cu successively, the maximum entropy generation values due to the heat transfer has increased gradually from 6044.07 to 6420.29. Moreover, both SVG and STG distributions illustrated symmetrical trend according to the vertical centreline independent from the applied nanofluid type. In the arrangement core of STG *iso*-contours, the distribution initiated in a plume-like manner from the spheres' tops. According to SVG contours, ring-like distributions have taken the place of spheres with the maximum values for the case of Cu nanoparticles.

In this section, the impact of Rayleigh number, volume fraction, and nanofluid type is discussed in terms of entropy generation. Results are illustrated in the form of entropy maps. The entropy contours for different values of Ra, volume fraction and nanoparticles type (CuO, Cu and Al_2O_3) have been presented in Figs. 6–11. It is a well-known fact that the irreversibilites produced by any thermal system hampers its theoretical efficiency, and hence, analysing the impact of different parameters on irreversibilities offers the opportunities to enhance the overall performance of thermal systems. The amount of irreversibilities is directly proportional to the entropy generation, and in buoyancy driven flows, the entropy generation is mainly due to the heat transfer and fluid-friction.

Figs. 6, 7 and 8 presents the isosurfaces of maximum local entropy generation contours due to friction irreversibilities $S^{max}_{VG,loc}$ of different nanofluids (CuO-water, Al_2O_3-water and Cu-water) with various volume fraction of nanoparticles (ϕ = 0.02, 0.04, 0.06 and 0.08) at the vertical plane (y, z) for Ra = 10^4, 10^5 and 10^6 successively. It is clear that the maximum values of local entropy generation due to friction are increasing by further increasing the volume fraction of nanoparticles from 2% to 8% regardless the type of nanofluid and Rayleigh number. Moreover, it is noted that the maximum values of local SVG corresponding to Cu are greater than those corresponding to CuO and those of CuO are greater than Al_2O_3 nanoparticles.

Figs. 9, 10 and 11 depict the entropy maps due to heat transfer $S^{max}_{TG,loc}$ of different nanofluids (CuO-water, Al_2O_3-water and Cu-water) with various volume fraction of nanoparticles (ϕ = 0.02, 0.04, 0.06 and 0.08) at the vertical plane (y, z) for Rayleigh numbers ranging from 10^4 to 10^6. Same behavior is observed here as observed in $S^{max}_{VG,loc}$ isocontours, where we note that it is clear that the maximum values of local entropy generation due to heat transfer are increasing by further increasing the volume fraction of nanoparticles from 2% to 8% regardless the type of nanofluid and Rayleigh number.

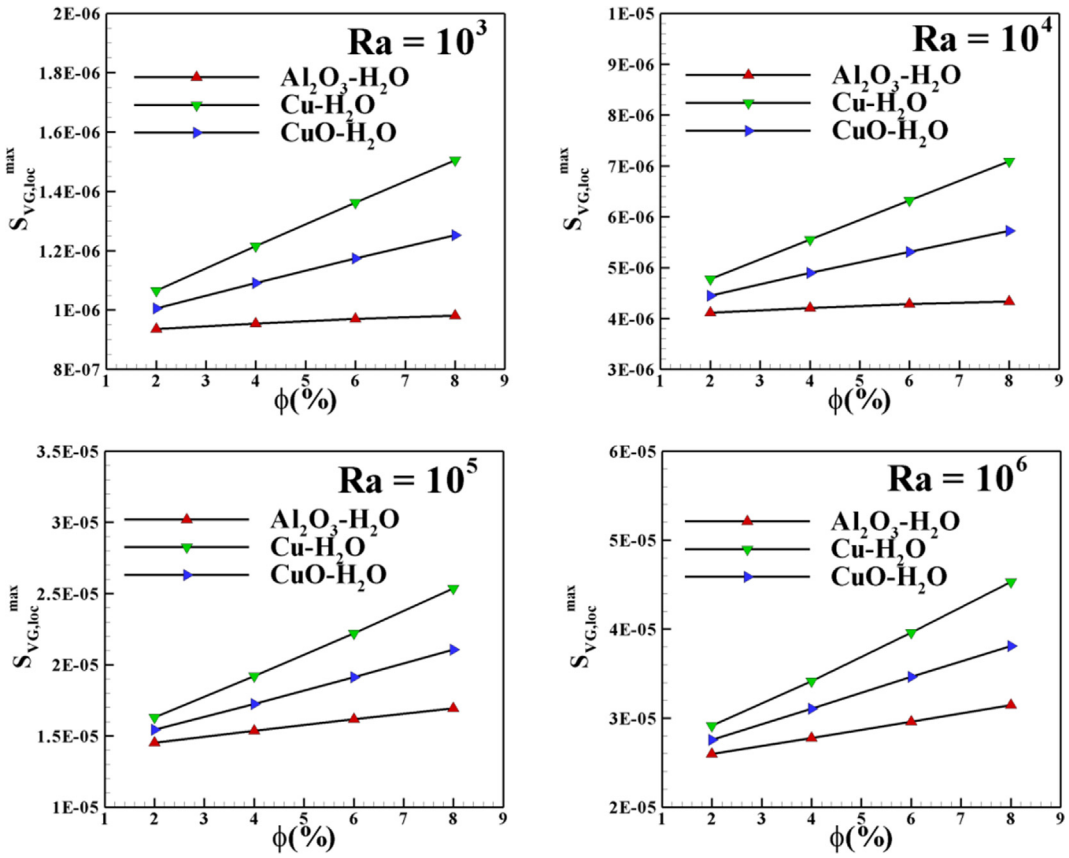

Fig. 12 Variation of maximum local entropy generation profiles due to friction $S^{max}_{VG,loc}$ of different nanofluids (CuO-water, Al_2O_3-water and Cu-water) versus the volume fraction of nanoparticles for Rayleigh numbers ranging from 10^3 to 10^6.

However, in this case it is noted that the maximum values of local STG corresponding to Cu are greater than those corresponding to Al_2O_3 and those of Al_2O_3 are greater than CuO nanoparticles for all Rayleigh numbers. Furthermore, it is seen that the entropy generation due to fluid-friction is negligible in comparison to the heat transfer at Rayleigh values 10^4, 10^5 and 10^6. Also, the entropy (STG) values are observed to be greater, and the maximum entropy generation occurs at the center of the spheres.

To sum up the section of entropy maps, past studies on the topic under investigation have demonstrated that the addition of nanoparticles to a base fluid (water) generates the occurrence of two opposing effects on the convective heat transfer within the horizontal arrangement induced by two spheres. The first effect, resulting from the enhanced thermal conductivity of the mixture owing to the presence of the nanoparticles, tends to increase $S^{max}_{TG,loc}$. The second effect, owing to the increase of viscosity caused by the nanoparticles, eliminates the convection motion and as a conclusion increases $S^{max}_{VG,loc}$. Thus, the current mechanism is monitored by the convection intensity (Rayleigh number value), type of the particles used and the models adopted to evaluate the viscosity and thermal conductivity of the mixture.

Fig. 12 shows the maximum local entropy generation due to friction $S^{max}_{VG,loc}$ versus the volume fraction of different nanofluids (CuO-water, Al_2O_3-water and Cu-water) for different Rayleigh numbers. As it can be seen from the figure, the entropy generation number increases as the volume fraction ϕ increase for all Rayleigh numbers. Also, the figure illustrates that the difference between the values of entropy generation number increases with increasing the Rayleigh number from 10^3 to 10^6. For instance, the $S^{max}_{VG,loc}$ is beyond 10^{-6} for Ra = 10^3 whereas it increases to 3.10^{-5} for a Rayleigh number equates 10^6. On the other hand, in accordance with the previous entropy maps presented in Figs. 6, 7 and 8, there is further evidence that the entropy generation due to fluid friction of the copper (Cu) are greater than the oxide copper (CuO) and the latter is great than aluminum oxide (Al_2O_3).

Fig. 13 displays the Variation of maximum local entropy generation profiles due to heat transfer $S^{max}_{TG,loc}$ of different nanofluids (CuO-water, Al_2O_3-water and Cu-water) versus the volume fraction of nanoparticles for Rayleigh numbers ranging from 10^3 to 10^6. As is well known, the increment in effective thermal conductivity of nanofluid with higher ϕ yields large thermal gradient, and hence, the irreversibility due to heat transfer augments. In this figure, the maximal local entropy generation due to heat transfer undergoes a slight increase of 5800 for a Rayleigh number 10^3 to 6000 for a Rayleigh number 10^6. Moreover, $S^{max}_{TG,loc}$ profiles are seen increasing monotonously by increasing the volume fraction for all Rayleigh numbers and nanoparticles. The maximal local entropy generation due to heat transfer is also organized according to the following order; CuO, Al_2O_3 and then Cu nanoparticles for Rayleigh numbers 10^4, 10^5 and 10^6. How-

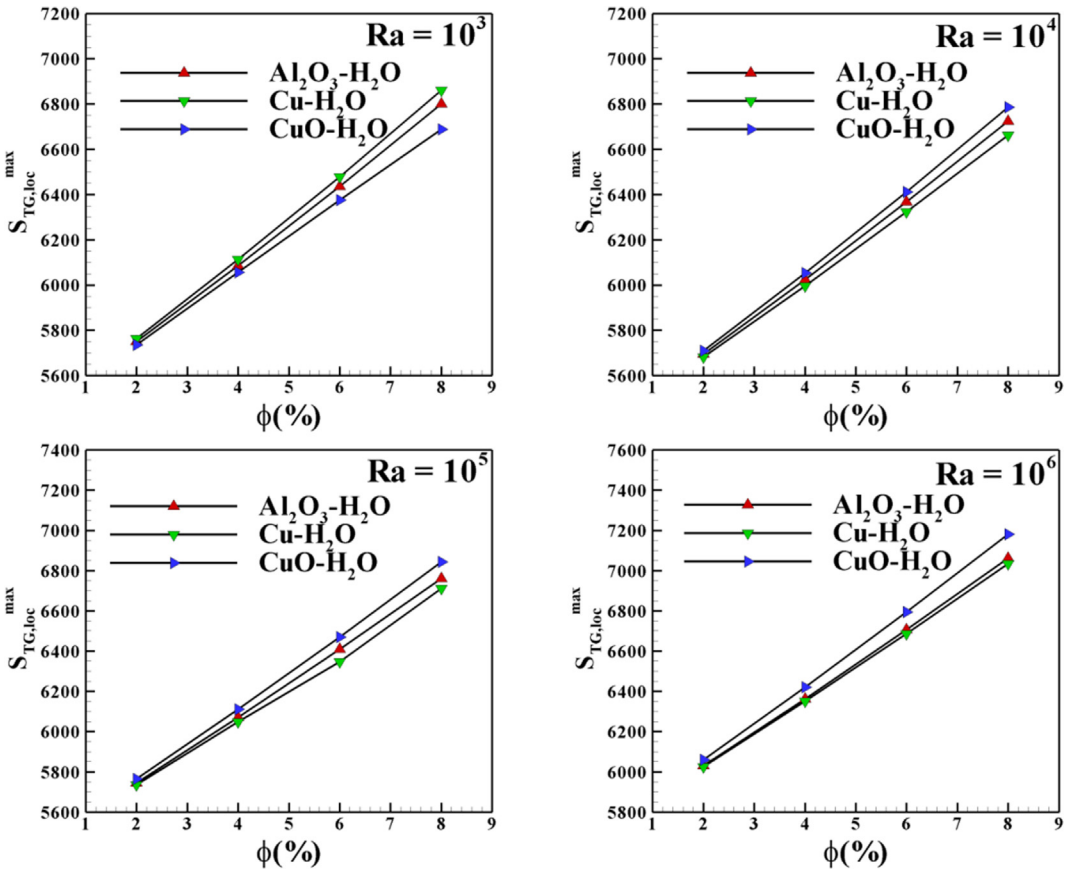

Fig. 13 Variation of maximum local entropy generation profiles due to heat transfer $S^{max}_{TG,loc}$ of different nanofluids (CuO-water, Al_2O_3-water and Cu-water) versus the volume fraction of nanoparticles for Rayleigh numbers ranging from 10^3 to 10^6.

ever, a different behavior is observed for Ra = 10^3, where we note that the maximal local entropy generation due to heat transfer of Cu is better than Al_2O_3, and the latter one is better than CuO nanoparticles.

Overall, at higher Ra values, the convection is dominant. Hence, the motion inside the cavity enhances and the entropy generation increases with a maximum rate obtained for a solid volume fraction $\phi = 0.08$. Loss of available energy is directly related to the total entropy generation which will be presented in the next section.

The dominance of thermal irreversibility and/or fluid-friction irreversibility on total entropy generation is quantified through mean Bejan number. If Be > 0.5, then the fluid-friction irreversibility is insignificant in comparison to the heat transfer irreversibility, and the value of Be less than 0.5 suggests that the dominance of fluid-friction irreversibility over thermal entropy generation. In the present study, Fig. 14 presents the Variation of Bejan number profiles of different nanofluids (CuO-water, Al_2O_3-water and Cu-water) versus Rayleigh numbers for different volume fraction of nanoparticles (ϕ = 0.02, 0.04, 0.06 and 0.08). For all the values of Φ, the Bejan number of Al_2O_3 nanoparticles is greater than those of CuO, and those of CuO are greater than Cu nanoparticles. Besides, the Be number is enhanced monotonously for Rayleigh numbers ranging from 10^3 to 10^5. However, for Ra = 10^5, we note a drop in the Bejan number for all volume fraction values and nanoparticle types.

4.3. Heat transfer characteristics

The influence of nanofluid volume fraction, Rayleigh number and nanoparticle type on mean Nusselt number of the horizontal plates of the arrangement has been presented in Fig. 15. It is clear that the increment in Ra enriches the heat transfer of a 57% (e. g. from 1.45 for a Rayleigh number 10^3 to 3.4 for a Rayleigh number 10^6) for ϕ = 2%. Obviously, quantitative influence of Ra and Φ varies notably. The thermal dissipation is insignificant while Ra value shifts from 10^3 to 10^4 for all the other parameters embraced in the study. This is due to the marginal convection of the fluid at $Ra = 10^4$ in comparison to higher Ra values, and therefore, the dissipation of heat is insignificant. Further enhancement of Rayleigh number results the prominent increment in $\bar{Nu}_{Plates}$ value. Also, the enhancement trend of $\bar{Nu}_{Plates}$ with ϕ for different values of Rayleigh number and all nanoparticles used in the study is observed to be notable. For aforementioned parameters, this suggests that the introduction of more nanoparticles is not affecting the thermal enhancement percentage with reference to buoy-

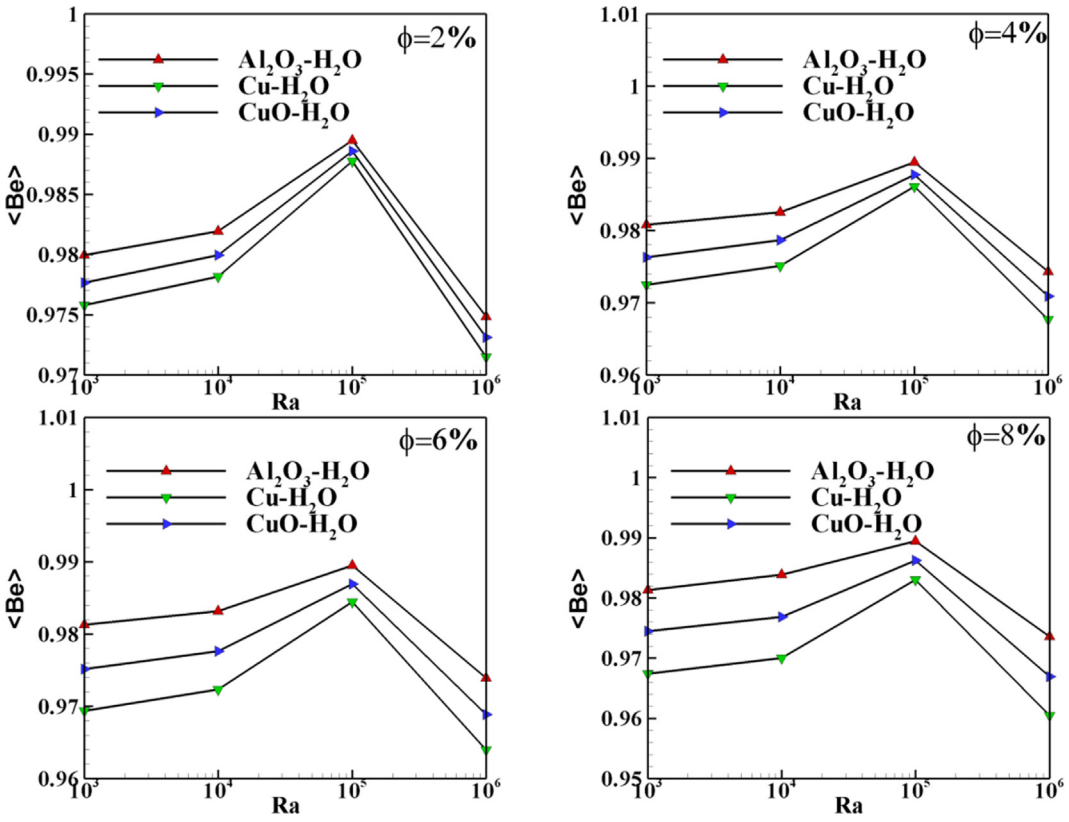

Fig. 14 Variation of Bejan number profiles of different nanofluids (CuO-water, Al_2O_3-water and Cu-water) versus Rayleigh numbers for different volume fraction of nanoparticles (ϕ = 0.02, 0.04, 0.06 and 0.08).

ancy force. It is to be noted that in the present investigation, elevating nanofluid volume fraction has shown marginal effect on fluid flow. Owing to this, inclusion of different nanoparticles has not shown significant heat transfer variation for Rayleigh numbers 10^3 and 10^4. Whereas, the variation is more important for Ra = 10^5 and 10^6. Furthermore, the mean Nusselt number of the plates corresponding to the copper is better than that of oxide aluminium which is also better than oxide copper for Ra = 10^3 to 10^4. Thus, for Ra = 10^5 and 10^6 there is a different trend between copper oxide and aluminium oxide.

A variation of the mean Nusselt number along the spheres for different nanofluids (CuO-water, Al_2O_3-water and Cu-water) versus the volume fractions at different Rayleigh numbers is shown in Fig. 16. As seen in this figure, increased volume fraction of nanofluid increased the Nusselt number of the left and right spheres for Rayleigh numbers taken from 10^3 to 10^6 and different nanoparticles, this is due to the fact that the increased concentration of nanofluid increases leading to the clustering phenomenon in the nanofluid. This phenomenon increases the thermal conductivity and convective heat transfer coefficient, as well as the heat transfer in the nanofluid. Furthermore, as shown in the plots of the same figure and for a fixed solid volume fraction ϕ = 2%, the mean Nusselt number of the spheres enhanced with 57.4% from Ra = 10^3 to Ra = 10^6 ($\bar{Nu}_{sp} = 8.52$ for Ra = 10^3 and $\bar{Nu}_{sp} = 20$for Ra = 10^6). Mean Nusselt numbers of the spheres are following a linear trend for all Rayleigh numbers and nanoparticles where profiles are almost confused for Ra = 10^3 and 10^4. However, profiles are distant for Ra = 10^5 and 10^6. Likewise the mean Nusselt number of the plates, here the mean Nusselt number of the spheres is following the same behaviour. For instance, according to Ra = 10^3 and 10^4 $(\bar{Nu}_{sp}(Cu) \succ \bar{Nu}_{sp}(Al_2O_3) \succ \bar{Nu}_{sp}(CuO)$. Thus, for Ra = 10^5 and 10^6, $\bar{Nu}_{sp}(Cu) \succ \bar{Nu}_{sp}(CuO) \succ \bar{Nu}_{sp}(Al_2O_3)$.

Indeed, as shown in Fig. 17, the values of the averaged Nusselt number whether through the channel walls (plates) or the spheres are higher when the nanofluid used is based C*u* nanoparticles. Fig. 17 also shows that the averaged Nusselt number for both cases can be correlated by equations of the form:

$$\bar{Nu}_{Plates} = 1.863 + 0.038 \times \phi$$

$$\bar{Nu}_{Sp} = 11.12 + 0.23 \times \phi$$

Previously, the ecological coefficient of performance (ECOP) has been defined as a criterion for evaluation of the performance of extended surfaces. In this section, ECOP for determination of the thermal performance of the horizontal arrangement is introduced. ECOP is based on the second law of thermodynamics and is defined as the ratio of the Nusselt number to entropy generation number. ECOP indicates indeed the ratio heat transfer rate to the total irreversibility rate, starts from zero and does not have an upper limit. Increasing the ECOP is desirable (this is similar to COP for a refrigerator, but COP is based on the first law of thermodynamics whereas ECOP is based on the second law of thermodynamics). ECOP can be defined as follow:

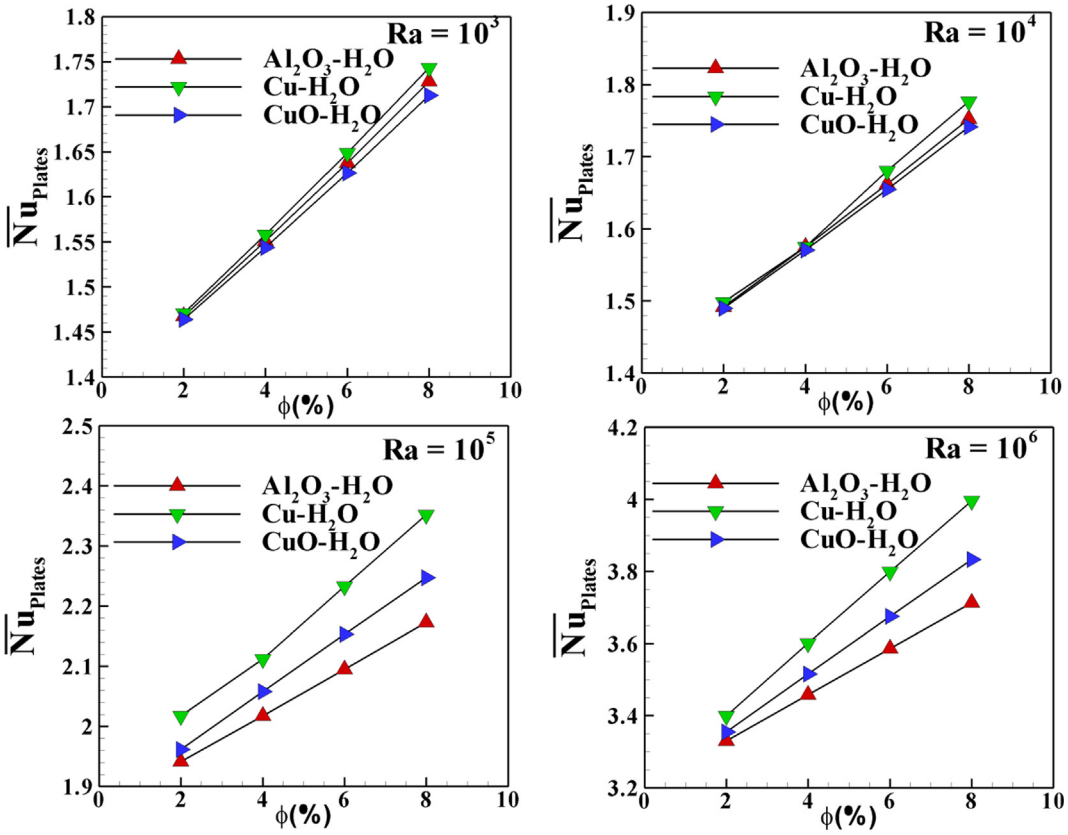

Fig. 15 Variation of the average Nusselt number profiles along the horizontal plates of different nanofluids (CuO-water, Al_2O_3-water and Cu-water) versus the volume fractions at different Rayleigh numbers.

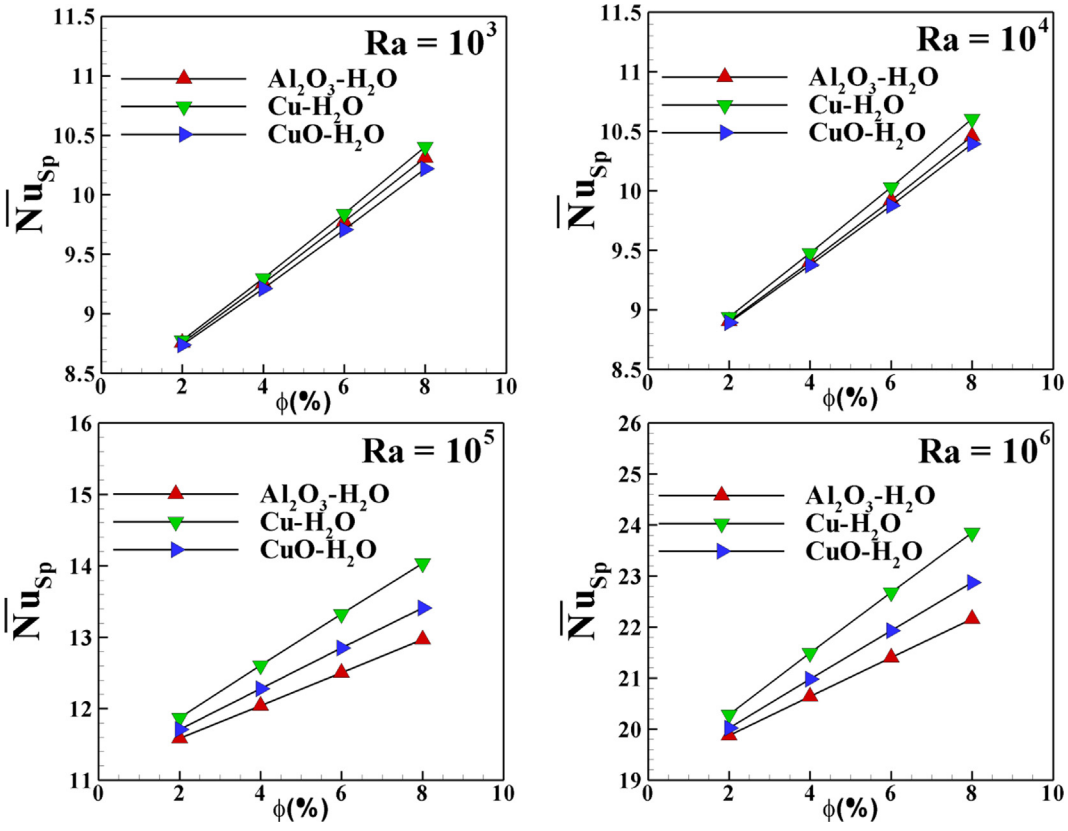

Fig. 16 Variation of the average Nusselt number profiles along the spheres of different nanofluids (CuO-water, Al_2O_3-water and Cu-water) versus the volume fractions at different Rayleigh numbers.

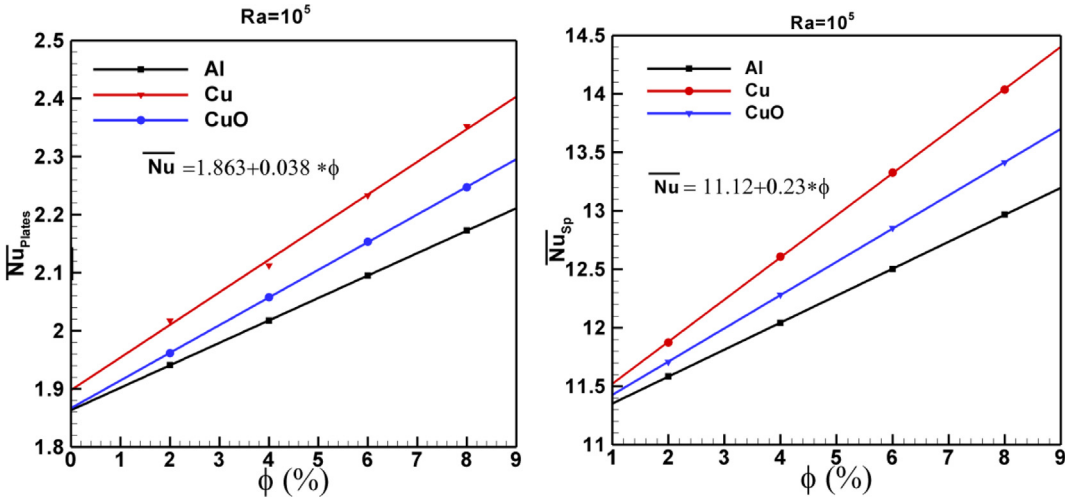

Fig. 17 Average Nusselt number through the channel walls (plates) and the spheres versus the volume fraction for the considered nanofluids at Ra = 10^5.

$$ECOP = \frac{\bar{N}u_{Plates}}{S_{tot}}$$

Herein, Fig. 18 displays the total entropy generation profiles (left) and the ecological coefficient of performance ECOP (right) versus the volume fractions of different nanofluids (CuO-water, Al_2O_3-water and Cu-water) for various Rayleigh numbers. Fig. 17 shows that the ECOP of CuO nanoparticles decreases as the volume fraction of nanoparticles increases for all Rayleigh numbers. Contrarily, it increases from 2.89 for a Rayleigh number equates 10^3 to 7.8 for a Rayleigh number equates 10^6 (63% enhancement) for ϕ = 2%. On the other hand, the total entropy generation increases as the volume fraction of nanoparticles increases for the considered Rayleigh numbers. As the total entropy generation increases, the required energy for heating the fluid decreases. This is due to the fact that, by increasing the total entropy generation, a major part of this was used to remove the irreversibilities rather than heating the fluid. As observed in Fig. 17, the total entropy generation is reduced with Ra. It is interesting to observe that, the overall heat transfer rate or the total entropy generation due to heat transfer augments with Ra and ϕ. This can be explained by the loss in available energy due to fluid friction irreversibilities.

5. Concluding remarks

In this study, the entropy generation of water-based nanofluids during natural convection in a horizontal arrangement was evaluated through numerical modelling. The entropy maps were utilized to indicate the generated entropy caused by irreversibility of the generated entropy as well as the fluid friction. Several nanofluids including Cu-water, CuO-water, and Al_2O_3-water with various volume fractions ranging from 0 to 8% were considered for these characterizations. A wide value ranges from 10^3 to 10^6 was also selected for the Rayleigh number. The impact of various parameters on STG and SVG were also investigated. Variation of several terms including the total entropy generation, average Bejan number, and ecological coefficient of performance were studied against Ra and ϕ factors. The obtained results could be summarized as follows:

- According to deformation of the viscous force and the isothermal line, Rayleigh number enhancement indicated strengthening of the buoyancy forces.
- Increment of the volume fraction led to improvement of the velocity components and so enhancement of the energy transport inside the fluid.
- Thermal conductivity enhancement of the applied nanofluids resulted in the sensitivity of thermal boundary layer thickness to the volume fraction.
- Volume fraction increment caused raising of the viscosity and thermal conductivity features of the various nanofluids and so improvement of the heat transfer rate.
- $S^{max}_{VG,loc}$ and $S^{max}_{TG,loc}$ increased by enhancing the values of Ra and ϕ.
- Cu nanoparticles have the higher heat transfer rates whether for the channel walls (plates) or the spheres in comparison with the other nanoparticles.
- Rate of the heat transfer as well as the generated entropy were influenced significantly by the applied nanoparticle type. Insertion of the Al_2O_3 nanoparticles into the water base fluid caused the highest Be of 0.98.
- The ECOP of CuO nanoparticles decreased as the volume fraction of nanoparticles increased for all Rayleigh numbers.
- All utilized nanoparticles showed raising of the average Nusselt number with increment of the volume fraction at all Rayleigh number values.
- The mean Nusselt numbers of the spheres and horizontal plates were increased to 57.4 by increment of the Ra from 10^3 to 10^6 at a constant volume fraction of 2%.

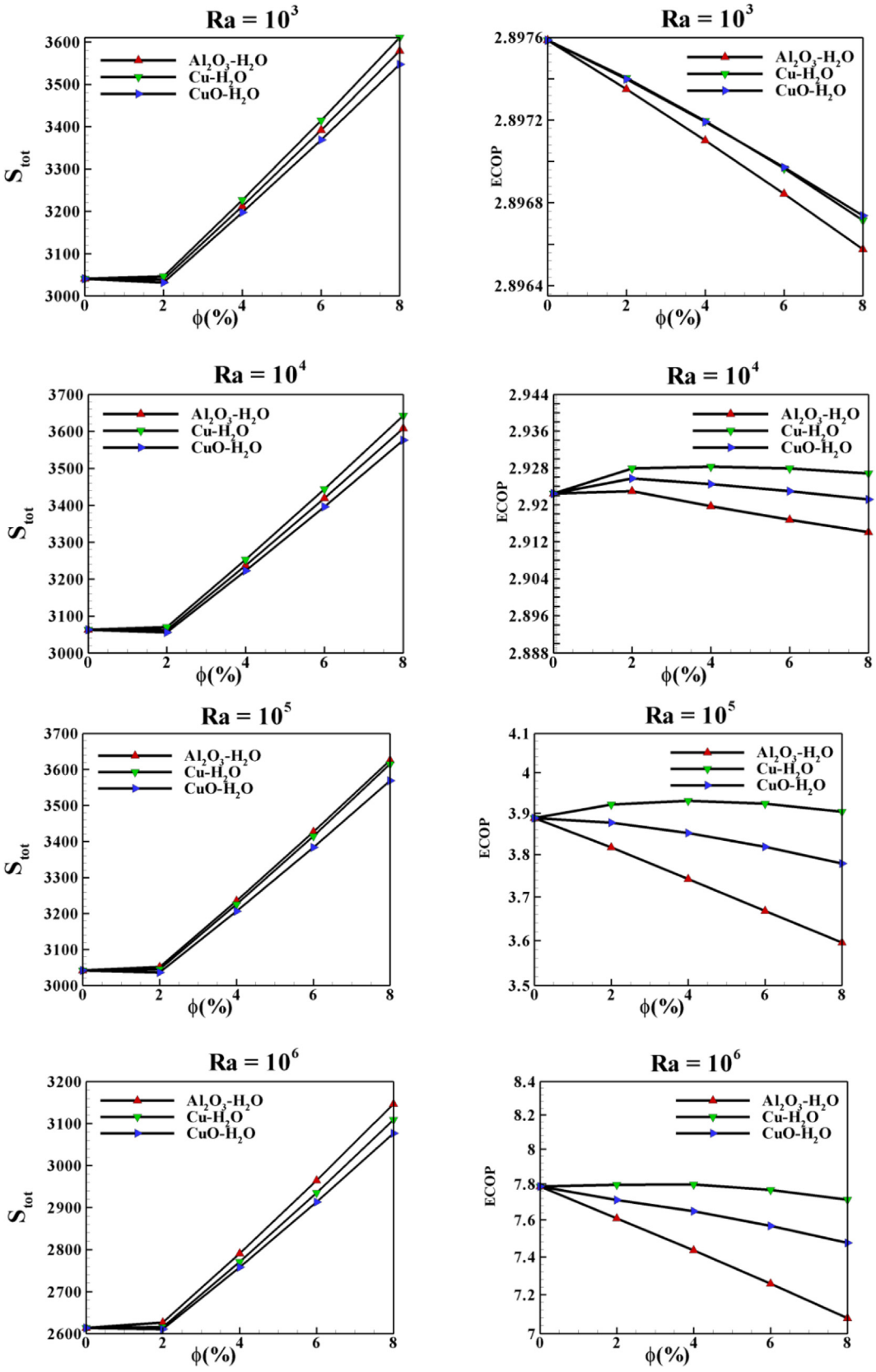

Fig. 18 Variation of the total entropy generation profiles (left) and ECOP (right) versus the volume fractions of different nanofluids (CuO-water, Al_2O_3-water and Cu-water) for various Rayleigh numbers.

Declaration of Competing Interest

The authors declare that they have no known competing financial interests or personal relationships that could have appeared to influence the work reported in this paper.

Acknowledgment

The authors gratefully acknowledge the Deanship of Scientific Research at King Faisal University for the financial support under Research Group Support Track (Grant No. 1811014).

References

[1] S. Kakac, A. Pramuanjaroenky, Review of convective heat transfer enhancement with nanofluids, Int. J. Heat Mass Transf. 52 (2009) 3187–3196.
[2] S. Kakac, A. Pramuanjaroenky, Single-phase and two-phase treatments of convective heat transfer enhancement with nanofluids- A state- of- the- art review, Int. J. Therm. Sci. 100 (2016) 75–97.
[3] A.A.A.A. Al-Rashed, W. Aich, L. Kolsi, O. Mahian, A.K. Hussein, M.N. Borjini, Effects of movable-baffle on heat transfer and entropy generation in a cavity saturated by CNT suspensions: Three dimensional modeling, ENTROPY 19 (2017) 200.
[4] A.A.A.A. Al-Rashed, K. Kalidasan, L. Kolsi, M.N. Borjini, P. Rajesh Kanna, Three dimensional natural convection of CNT-water nanofluid confined in an inclined enclosure with Ahmed body, J. Therm. Sci. Technol. 12 (1) (2017) JTST0002.
[5] L. Kolsi, E. Lajnef, W. Aich, A. Alghamdi, M.A. Aichouni, M. N. Borjini, H. Ben Aissia, Numerical investigation of combined buoyancy-thermocapillary convection and entropy generation in 3D cavity filled with Al2O3 nanofluid, Alexandria Eng. J. 56 (2017) 71–79.
[6] L. Kolsi, H.F. Oztop, A. Alghamdi, N. Abu-Hamdeh, M.N. Borjini, H. Ben Aissia, A computational work on three dimensional analysis of natural convection and entropy generation in nanofluid filled enclosures with triangular solid insert at the corners, J. Mol. Liq. 218 (2016) 260–274.
[7] L. Kolsi, O. Mahian, H.F. Oztop, W. Aich, M.N. Borjini, N. Abu-Hamdeh, H. Ben Aissia, 3D Buoyancy induced flow and entropy generation of nanofluid filled open cavity having adiabatic diamond shaped obstacle, ENTROPY 18 (6) (2016) 232.
[8] L. Kolsi, K. Kalidasan, A. Alghamdi, M.N. Borjini, P.R. Kanna, Natural convection and entropy generation on a cubical cavity with twin adiabatic blocks and filled by aluminium oxide-water nanofluid, Numer. Heat Transfer, Part A 70 (3) (2016) 242–259.
[9] L. Kolsi, A.K. Hussein, M.N. Borjini, H.A. Mohammed, H. Ben Aïssia, Computational analysis of three-dimensional unsteady natural convection and entropy generation in a cubical enclosure filled with water-Al2O3 nanofluid, Arabian J. Sci. Eng. 39 (2014) 7483–7493.
[10] B. Singh, S.K. Dash, Natural convection heat transfer from a finned sphere, Int. J. Heat Mass Transfer 81 (81) (2015) 305–324.
[11] O.G. Martynenko, P.P. Khramtsov, Free-Convective Heat Transfer: With Many Photographs of Flows and Heat Exchange, Springer Science & Business Media, 2005.
[12] S. Yamoah, E.H. Akaho, N.G. Ayensu, et al, Analysis of fluid flow and heat transfer model for the pebble bed high temperature gas cooled reactor, Res. J. Appl. Sci. Eng. & Tech. 4 (12) (2012) 1659–1666.
[13] Y. Lei, W.L. Zhan, New concept for ADS spallation target: gravity-driven dense granular flow target, Sci. China Technol. Sc. 58 (10) (2015) 1705–1711.
[14] M. Sheikholeslami, S.A. Shehzad, Zhixiong Li, Water based nanofluid free convection heat transfer in a three dimensional porous cavity with hot sphere obstacle in existence of Lorenz forces, Int. J. Heat Mass Transf. 125 (2018) 375–386.
[15] Mohammed Z. Swalmeh, Hamzeh T. Alkasasbeh, Abid Hussananan, Mustafa Mamat, Heat transfer flow of Cu-water and AL2O3-Water micropolar nanofluids about a solid sphere in the presence of natural convection using Keller-Box method, Results Phys. 9 (2018) 717–724.
[16] Firas A. Alwawi, Hamzeh T. Alkasasbeh, A.M. Rashad, Ruwaidiah Idris, MHD natural convection of sodium alginate Casson nanofluid over a solid sphere, Results Phys. (2019), https://doi.org/10.1016/j.rinp.2019.102818.
[17] A. Baïri, Using nanofluid saturated porous media to enhance free convective heat transfer around a spherical electronic device, Chin. J. Phys. (2020), https://doi.org/10.1016/j.cjph.2020.03.023.
[18] Anoop K. Gupta, Garima Mishra, N. Nirmalkar, R.P. Chhabra, Effect of confinement on heat transfer in aqueous nanofluids from a heated sphere, Powder Technol. 325 (2018) 576–596.
[19] Shu Yang, Vasudevan Raghavan, George Gogos, Numerical study of transient laminar natural convection over an isothermal sphere, Int. J. Heat Fluid Flow 28 (4) (2007) 821–837.
[20] Nepal C. Roy, M.A. Hossain, R.S.R. Gorla, Unsteady free convection from a heated sphere in the presence of internal heat generation or absorption, Int. J. Therm. Sci. 98 (2015) 237–244.
[21] Daehoon Lee, Hosung Jang, Byeong Jun Lee, Wonjoon Choi, Chan Byon, Internal natural convection around a sphere in a rectangular chamber, Int. J. Heat Mass Transf. 136 (2019) 501–509.
[22] K. Kitamura, A. Mitsuishi, T. Suzuki, T. Misumi, Fluid flow and heat transfer of high-Rayleigh-number natural convection around heated spheres, Int. J. Heat Mass Transf. 86 (2015) 149–157.
[23] M. Zaydan, A. Wakif, I.L. Animasaun, Umair Khan, Dumitru Baleanu, R. Sehaqui, Significances of blowing and suction processes on the occurrence of thermo-magneto-convection phenomenon in a narrow nanofluidic medium: A revised Buongiorno's nanofluid model, Case Stud. Therm. Eng. 22, 100726 (2020).
[24] Abderrahim Wakif Zoubair, Boulahia Rachid Sehaqui, Numerical analysis of the onset of longitudinal convective rolls in a porous medium saturated by an electrically conducting nanofluid in the presence of an external magnetic field, Results Phys. 7 (2017) 2134–2152.
[25] Abderrahim Wakif Zoubair, Boulahia Rachid Sehaqui, A semi-analytical analysis of electro-thermo-hydrodynamic stability in dielectric nanofluids using Buongiorno's mathematical model together with more realistic boundary conditions, Results Phys. 9 (2018) 1438–1454.
[26] Muhammad Usman Ashraf, Muhammad Qasim, Abderrahim Wakif, Muhammad Idrees Afridi, Isaac L. Animasaun, A generalized differential quadrature algorithm for simulating magnetohydrodynamic peristaltic flow of blood-based nanofluid containing magnetite nanoparticles: A physiological application, https://doi.org/10.1002/num.22676 (2020).
[27] A. Wakif, I.L. Animasaun, P.V. Satya Narayana, G. Sarojamma, Meta-analysis on thermo-migration of tiny/nano-sized particles in the motion of various fluids, Chin. J. Phys. 68 (2020) 293–307.
[28] Abderrahim Wakif, Zoubair Boulahia, S.R. Mishra, Mohammad Mehdi Rashidi, Rachid Sehaqui, Influence of a uniform transverse magnetic field on the thermo-hydrodynamic stability in water-based nanofluids with metallic nanoparticles

using the generalized Buongiorno's mathematical model, Eur. Phys. J. Plus 133 (2018) 181.
[29] Abderrahim Wakif, Zoubair Boulahia, Farhad Ali, Mohamed R. Eid, Rachid Sehaqui, Numerical analysis of the unsteady natural convection MHD Couette nanofluid flow in the presence of thermal radiation using single and two-phase nanofluid models for Cu–water nanofluids, Int. J. Appl. Computat. Math. 4 (2018) 81.
[30] Abderrahim Wakif, Ali Chamkha, Thirupathi Thumma, I.L. Animasaun, Rachid Sehaqui, Thermal radiation and surface roughness effects on the thermo-magneto-hydrodynamic stability of alumina–copper oxide hybrid nanofluids utilizing the generalized Buongiorno's nanofluid model, J. Therm. Anal. Calorim. (2020), https://doi.org/10.1007/s10973-020-09488-z.
[31] Ahmed Kadhim Hussein, Hamid Reza Ashorynejad, Mohsen Shikholeslami, S. Sivasankaran, Lattice Boltzmann simulation of natural convection heat transfer in an open enclosure filled with Cu–water nanofluid in a presence of magnetic field, Nucl. Eng. Des. 268 (2014) 10–17.
[32] Ahmed Kadhim Hussein, Salam Hadi Hussain, Heatline visualization of natural convection heat transfer in an inclined wavy cavities filled with nanofluids and subjected to a discrete isoflux heating from its left sidewall, Alexandria Eng. J. 55 (2016) 169–186.
[33] Z.A.S. Raizah, Abdelraheem M. Aly, Sameh E. Ahmed, Natural convection flow of a power-law non-Newtonian nanofluid in inclined open shallow cavities filled with porous media, Int. J. Mech. Sci. 140 (2018) 376–393.
[34] A.A. Abdullah, A. Al-Rashed, K. Kalidasan, Lioua Kolsi, Abdelkarim Aydi, Emad Hasani Malekshah, Ahmed Kadhim Hussein, P. Rajesh Kanna, Three-dimensional investigation of the effects of external magnetic field inclination on laminar natural convection heat transfer in CNT–water nanofluid filled cavity, J. Mol. Liquids 252 (2018) 454–468.
[35] Z. Li, A.K. Hussein, O. Younis, S. Rostami, W. He, Effect of alumina nano-powder on the natural convection of water under the influence of a magnetic field in a cavity and optimization using RMS: Using empirical correlations for the thermal conductivity and a sensitivity analysis, Int. Commun. Heat Mass Transfer 112 (2020) 104497.
[36] Z. Li, A.K. Hussein, O. Younis, M. Afrand, S. Feng, Natural convection and entropy generation of a nanofluid around a circular baffle inside an inclined square cavity under thermal radiation and magnetic field effects, Int. Commun. Heat Mass Transfer 116 (2020) 104650.
[37] Ahmad Hajatzadeh Pordanjani, Saeed Aghakhani, Abdulwahab A. Alnaqi, Masoud Afrand, Effect of alumina nano-powder on the convection and the entropy generation of water inside an inclined square cavity subjected to a magnetic field: Uniform and non-uniform temperature boundary conditions, Int. J. Mech. Sci. 152 (2019) 99–117.
[38] Dhrubajyoti Kashyap, Anoop K. Dass, Effect of boundary conditions on heat transfer and entropy generation during two-phase mixed convection hybrid Al2O3-Cu/water nanofluid flow in acavity, Int. J. Mech. Sci. 157–158 (2019) 45–59.
[39] Mehdi VahabzadehBozorg, Majid Siavashi, Two-phase mixed convection heat transfer and entropy generation analysis of a non-Newtonian nanofluid inside a cavity with internal rotating heater and cooler, Int. J. Mech. Sci. 151 (2019) 842–857.
[40] A.A.A.Abdullah Al-Rashed, Investigating the effect of alumina nanoparticles on heat transfer and entropy generation inside a square enclosure equipped with two inclined blades under magnetic field, Int. J. Mech. Sci. 152 (2019) 312–328.
[41] Wi Liu, Amin Shahsavar, Azeez A. Barzinjy, Abdullah A.A.A. Al-Rashed, Masoud Afrand, Natural convection and entropy generation of a nanofluid in two connected inclined triangular enclosures under magnetic field effects, Int. Commun. Heat Mass Transfer 108 (November 2019).
[42] Fatih Selimefendigil, Hakan F. Öztop, Effects of conductive curved partition and magnetic field on natural convection and entropy generation in an inclined cavity filled with nanofluid, Physica A 540 (2020).
[43] C. Sivaraj, M.A. Sheremet, MHD natural convection and entropy generation of ferrofluids in a cavity with a non-uniformly heated horizontal plate, Int. J. Mech. Sci. 149 (2018) 326–337.
[44] Basma Souayeh, Najib Hdhiri, Mir-Waqas Alam, Fayçal Hammami, Hu.da. Alfannakh, Convective heat transfer and entropy generation around a sphere within Cuboidal enclosure, J. Thermophys. Heat Transfer (2020), https://doi.org/10.2514/1.T5960.
[45] D.L. Brown, R. Cortez, M.L. Minion, Accurate projection methods for the incompressible NaviereStokes equations, J. Comput. Phys. 168 (2001) 464–499.
[46] T. Hayase, J.A.C. Humphrey, R. Greif, A consistently formulated QUICK scheme for fast and stable convergence using finite-volume iterative calculation procedures, J. Comput. Phys. 98 (1992) 108–118.
[47] R. Barrett, Templates for the Solution of Linear Systems: Building Blocks for Iterative Methods, Philadelphia SIAM Press, 1994.
[48] N. Ben-Cheikh, B. Ben-Beya, T. Lili, Benchmark solution for time-dependent natural convection flows with an accelerated full-multigrid method, Numer. Heat Transf. B 52 (2007) 131–151.
[49] Fayçal Hammami, Basma Souayeh, Nader Ben-Cheikh, Brahim Ben-Beya, Computational analysis of fluid flow due to a two-sided lid driven cavity with a circular cylinder, Comput. Fluids 156 (2017) 317–328.
[50] Basma Souayeh, Nader Ben-Cheikh, Brahim Ben-Beya, Numerical simulation of three-dimensional natural convection in a cubic enclosure induced by an isothermally-heated circular cylinder at different inclinations, Int. J. Therm. Sci. 10 (2016) 325–339.
[51] Sonia Bezi, Basma Souayeh, Nader Ben-Cheikh, Brahim Ben-Beya, Numerical simulation of entropy generation due to unsteady natural convection in a semi-annular enclosure filled with nanofluid, Int. J. Heat Mass Transf. 124 (2018) 841–859.
[52] Basma Souayeh, Fayçal Hammami, Najib Hdhiri and Huda Alfannakh, Unsteady state fluid structure of two-sided nonfacing lid-driven cavity induced by a semicircle at different radii sizes and velocity ratios, International Journal of Modern Physics C, Vol. 30, No. 8, 1950060 (33 pages), DOI: 10.1142/S0129183119500608 (2019).
[53] Faicel Hammami, Basma Souayeh, Nader Ben-Cheikh, Brahim Ben-Beya, Combined effects of the velocity and the aspect ratios on the bifurcation phenomena in a two-sided lid driven cavity flow, Int. J. Numer. Meth. Heat Fluid Flow (2018), https://doi.org/10.1108/HFF-09-2016-0361.
[54] Basma Souayeh, Flow instability of cylinder embedded within two-parallel moving walls of cuboidal cavity at different radii sizes, International Journal of Modern Physics C, Vol. 31, No. 5 (2020) 2050063 (24 pages), DOI: 10.1142/S0129183120500631 (2020).
[55] B.C. Pak, Y.I. Cho, Hydrodynamic and heat transfer study of dispersed fluids with submicron metallic oxide particles, Exp. Heat Transfer Int. J. 11 (1998) 151–170.
[56] Y. Xuan, W. Roetzel, Conceptions for heat transfer correlation of nanofluids, Int. J. Heat Mass Transf. 43 (2000) 3701–3707.
[57] R. Hamilton, O. Crosser, Thermal conductivity of heterogeneous two component systems, Indus. Eng. Chem. Fund. 1 (1962) 187–191.
[58] J. Maxwell, A Treatise on Electricity and Magnetism, second ed., Oxford University Press, Cambridge, UK, 1904.
[59] H.C. Brinkman, The viscosity of concentrated suspensions and solutions, J. Chem. Phys. 20 (1952) 571.

[60] K. Khanafer, K. Vafai, M. Lightstone, Buoyancy-driven heat transfer enhancement in a two-dimensional enclosure utilizing nanofluids, Heat Mass Transfer 46 (2003) 3639–3653.
[61] M.A. Rosen, Second-law analysis: approach and implications, Int. J. Energy Res. 33 (1999) 415–429.
[62] A. Bejan, A second-law analysis in heat transfer, Energy 5 (1980) 721–732.
[63] A. Bejan, Entropy Generation through Heat and Fluid Flow, Wiley, New York, 1982.
[64] W.M. El-Maghlany, K.M. Saqr, M.A. Teamah, Numerical simulations of the effect of an isotropic heat field on the entropy generation due to natural convection in a square cavity, Energy Convers. Mange. 85 (2014) 333–342.
[65] U. Narusawa, The second-law analysis of mixed convection in rectangular ducts, Heat Mass Transfer 37 (2001) 197–203.
[66] A.C. Baytas, Entropy generation for natural convection in an inclined porous cavity, Int. J. Heat Mass Transfer 43 (2000) 2089–2099.
[67] U. Narusawa, The second-law analysis of convective pattern change in a rectangular cavity, J. Fluid Mech. 392 (1999) 361–377.
[68] G.G. Ilis, M. Mobedi, B. Sunden, Effect of aspect ratio on entropy generation in a rectangular cavity with differentially heated vertical walls, Int. Commun. Heat Mass Transfer 35 (2008) 696–703.
[69] H.S. Yoon, D.H. Yu, M.Y. Ha, Y.G. Park, Three-dimensional natural convection in an enclosure with a sphere at different vertical locations, Int. J. Heat Mass Transf. 53 (2010) 3143–3155.
[70] Yosef Gulberg, Yuri Feldman, On laminar natural convection inside multi-layered spherical shells, Int. J. Heat Mass Transf. 91 (2015) 908–921.